

# **OMEN-SED 1.0: A new, numerically efficient sediment module for the coupling to Earth System Models**

Dominik Hülse<sup>1</sup>, Sandra Arndt<sup>1,2</sup>, Stuart Daines<sup>3</sup>, Andy Ridgwell<sup>1,4</sup>, and Pierre Regnier<sup>2</sup>

<sup>1</sup>School of Geographical Sciences, University of Bristol, Clifton, Bristol BS8 1SS, UK

<sup>2</sup>Department of Earth and Environmental Sciences, Université Libre de Bruxelles, Brussels, Belgium

<sup>3</sup>Earth System Science, University of Exeter, North Park Road, Exeter EX4 4QE, UK

<sup>4</sup>Department of Earth Sciences, University of California, Riverside, CA 92521, USA

*Correspondence to:* Dominik Hülse (Dominik.Huelse@bristol.ac.uk)

**Abstract.** Here we describe the first version of the Organic Matter ENabled SEDiment model (OMEN-SED 1.0).

## Contents

	<b>1 Introduction</b>	<b>3</b>
5	<b>2 Model Description</b>	<b>7</b>
	2.1 General Model Approach . . . . .	7
	2.2 Transport . . . . .	9
	2.3 Reaction Network . . . . .	10
	2.3.1 Organic matter or Particulate Organic Carbon (POC) . . . . .	10
10	2.3.2 Oxygen . . . . .	11
	2.3.3 Nitrate and Ammonium . . . . .	12
	2.3.4 Sulfate and Sulfide . . . . .	13
	2.3.5 Phosphate . . . . .	14
	2.3.6 Dissolved Inorganic Carbon (DIC) . . . . .	17
15	2.3.7 Alkalinity . . . . .	18
	2.4 Model Parameters . . . . .	19
	2.4.1 Transport Parameters . . . . .	19
	2.4.2 Reaction Parameters and Stoichiometries . . . . .	21
	2.5 Module Structure . . . . .	21
20	2.5.1 Generic Boundary Condition Matching (GBCM) . . . . .	21
	2.5.2 Coupling to an Earth System Model . . . . .	26
	<b>3 Model Applications</b>	<b>28</b>
	3.1 Sediment profiles . . . . .	28
	3.2 Sensitivity Analysis . . . . .	30
25	3.3 Pre-industrial cGENIE coupling and the OM degradation rate . . . . .	32
	<b>4 Scope of applicability and model limitations</b>	<b>35</b>
	<b>5 Conclusions</b>	<b>37</b>
	<b>6 Code Availability</b>	<b>37</b>
	<b>A Reaction Network</b>	<b>37</b>
30	<b>B Sensitivity Analysis</b>	<b>37</b>
	B1 . . . . .	39

## 1 Introduction

**DH:** How to include comments.

### **Role of marine sediments for climate and global biogeochemical cycles:**

Marine surface sediments are key components in the Earth system. They host the largest carbon  
35 reservoir within the surficial Earth system, provide the only long term sink for atmospheric CO<sub>2</sub>,  
recycle nutrients and represent the most important geochemical archive used for deciphering past  
changes in biogeochemical cycles and climate (e.g. Berner, 1991; Archer and Maier-Reimer, 1994;  
Ridgwell and Zeebe, 2005; Arndt et al., 2013). Physical and chemical processes in sediments (i.e.  
diagenetic processes) depend on the water column and vice versa: Diagenesis is mainly donor con-  
40 trolled, as it is fuelled by the external supply of solid material (e.g. organic matter, calcium carbon-  
ate, opal) from the water column and is affected by overlying bottom water concentrations of solutes.  
At the same time, diagenesis in the sediments transforms the deposited material and returns some  
of the resulting products (e.g. nutrients, DIC) to the water column. This so-called benthic-pelagic  
coupling is essential for understanding global biogeochemical cycles and climate (e.g. Archer and  
45 Maier-Reimer, 1994; Archer et al., 2000; Soetaert et al., 2000; Mackenzie, 2005).

Biological primary production of organic matter (OM, CH<sub>2</sub>O in equation R1) and the reverse  
process of degradation can be written in a greatly simplified reaction as:



On geological timescales production of OM is generally greater than degradation which results in  
50 some organic matter being buried in marine sediments and oxygen accumulating in the atmosphere.  
Thus burial of OM leads to net oxygen input to, and CO<sub>2</sub> removal from the atmosphere (Berner,  
2004). On shorter timescales, the upper few meters of the sediments (i.e. early diagenesis) are specif-  
ically important as it is decided here if a substance is recycled to the water column or buried for a  
longer period of time in the deeper sediments (Hensen et al., 2006). Most biogeochemical cycles  
55 and reactions in this part of marine sediments can be related either directly or indirectly to the  
degradation of organic matter (e.g. Boudreau and Ruddick, 1991; Arndt et al., 2013). Organic matter  
degradation releases metabolic CO<sub>2</sub> to the pore water, causing it to have a lower pH and provoking  
the dissolution of CaCO<sub>3</sub> (Emerson and Bender, 1981). Oxygen and nitrate for instance, the most  
powerful electron acceptors, are consumed in the course of the degradation of organic matter, result-  
60 ing in the release of ammonium and phosphorous to the pore water. As such, degradation of OM in  
the sediments can profoundly affect the oxygen and nutrient inventory of the ocean and thus primary  
productivity (Van Cappellen and Ingall, 1994; Lenton and Watson, 2000).

Nutrient recycling from marine sediments has been suggested to play a key role for climate and  
ocean biogeochemistry for different events during Earth history. For example, feedbacks between  
65 phosphorous storage and erosion from shelf sediments and marine productivity have been hypoth-  
esised to play an important role for glacial/interglacial atmospheric CO<sub>2</sub> changes (Broecker, 1982;  
Ruttenberg, 1993). Furthermore, nutrient recycling from anoxic sediments has been invoked to ex-

plain the occurrence of more extreme events in Earth history, for instance Oceanic Anoxic Events (OAEs, e.g. Mort et al., 2007; Tsandev and Slomp, 2009). OAEs represent severe disturbances of the global carbon, oxygen and nutrient cycles of the ocean and are usually characterized by widespread bottom water anoxia and photic zone euxinia (Jenkyns, 2010). One way to explain the genesis and persistence of OAEs is increased oxygen demand due to enhanced primary productivity. Increased nutrient inputs to fuel primary productivity may have come from marine sediments as the burial efficiency of phosphorus declines when bottom waters become anoxic (Ingall and Jahnke, 1994; Van Cappellen and Ingall, 1994). The recovery from OAE like conditions is thought to involve the permanent removal of excess CO<sub>2</sub> from the atmosphere and ocean by burying carbon in the form of organic matter in marine sediments (e.g. Arthur et al., 1988; Jarvis et al., 2011), which is consistent with the geological record of widespread black shale formation (Stein et al., 1986). However, the overall amount, exact timing and the rate of organic matter burial remain a topic of an ongoing debate.

### **Diagenetic Models:**

Therefore, globally quantifying the burial and degradation of organic matter in marine sediments and related biogeochemical dynamics is important for understanding climate and the cycling of many chemical elements on various timescales. Such studies and quantifications are possible through the application of idealised mathematical representations of diagenesis, or so-called diagenetic models (see e.g. Berner, 1980; Boudreau, 1997). The number of research questions that can be addressed with diagenetic models is infinite and a plethora of different approaches have been developed, mainly following two distinct directions (Arndt et al., 2013).

First, state-of-the art vertically resolved diagenetic models simulating the entire suite of the essential coupled redox and equilibrium reactions within marine sediments that control carbon burial and benthic recycling fluxes (e.g. BRNS, Aguilera et al., 2005; CANDI, Boudreau, 1996; MEDIA, Meysman et al., 2003; STEADYSED, Van Cappellen and Wang, 1996). These “complete”, non-steady-state models, thus resolve the resulting characteristic redox-zonation of marine sediments through explicitly including oxic OM degradation, denitrification, oxidation by manganese and iron (hydr)oxides, sulphate reduction and methanogenesis as well as the reoxidation of reduced byproducts formed in the mineralization of OM (i.e. NH<sub>4</sub>, Mn<sup>2+</sup>, Fe<sup>2+</sup>, H<sub>2</sub>S, CH<sub>4</sub>). Furthermore, they incorporate various mineral dissolution and precipitation reactions, as well as fast equilibrium sorption processes for example of NH<sub>4</sub>, PO<sub>4</sub> and metal ions (i.e. Mn<sup>2+</sup>, Fe<sup>2+</sup> and Mg<sup>2+</sup>, compare Van Cappellen and Wang, 1996; Meysman et al., 2003). Modelled, depth-dependent, transport processes usually comprise advection, diffusion, bioturbation and bio-irrigation. This group of diagenetic models generally uses a so-called multi-G approach (Jørgensen, 1978; Berner, 1980), thus dividing the bulk organic carbon pool into a number of compound classes that are characterised by different degradabilities  $k_i$ , which are generally dependent on the type and concentration of the specific terminal electron acceptor (TEA). Due to the large number of interrelated processes and depth-

105 dependent parameters this group of diagenetic models needs to be solved numerically, thus resulting  
in a very high computational demand. These complex models have a great potential for quantifying  
OM degradation dynamics for sites where enough observations are available to constrain its model  
parameters (see e.g. Boudreau et al., 1998; Wang and Van Cappellen, 1996; Thullner et al., 2009,  
for applications). However, their suitability for coupling to an Earth system model (ESM) and their  
110 global applicability is limited by the high computation cost and the limited transferability of these  
model parameters from one site to the global scale (Arndt et al., 2013).

The second group of diagenetic models is less sophisticated and comprehensive than the “com-  
plete” diagenetic models and is used for the coupling to global ESMs (e.g. HAMOCC and NorESM  
use the model of Heinze et al. (1999)) or box models (e.g. DCESS, Shaffer et al., 2008 or MBM  
115 using MEDUSA, Munhoven, 2007). These analytic or semi-analytical models account for the most  
important transport processes (i.e advection, bioturbation and molecular diffusion) through basic  
parametrizations and include fewer biogeochemical reactions which are generally restricted to the  
upper, bioturbated 10 cm of the sediments. They assume that the sedimentary organic matter pool  
is composed of just a single compound class which is either degraded with a globally invariant  
120 degradation rate constant (Munhoven, 2007) or a fixed rate constant depending on local oxygen con-  
centrations (Shaffer et al., 2008; Palastanga et al., 2011). Pore water tracers explicitly represented in  
DCESS (Shaffer et al., 2008) and the HAMOCC model of Heinze et al. (1999) and Palastanga et al.  
(2011) are restricted to DIC, TA,  $\text{PO}_4$  and  $\text{O}_2$ . The MEDUSA model (Munhoven, 2007) considers  
 $\text{CO}_2$ ,  $\text{HCO}_3^-$ ,  $\text{CO}_3^{2-}$  and  $\text{O}_2$ . Other species produced or consumed during OM degradation are ne-  
125 glected. Thus, with oxygen being the only TEA explicitly modelled the influence of reduced species  
is only implicitly included in the boundary conditions for  $\text{O}_2$ . Newer versions of the HAMOCC  
model, being notable exceptions, as Ilyina et al. (2013) include  $\text{NO}_3$  and denitrification explicitly  
and the version of Palastanga et al. (2011) represents an explicit sedimentary phosphorus cycle. Sec-  
ondary redox reactions involving reduced substances or sorption processes are not included in any  
130 of the discussed models.

#### **How are sediments resolved in Earth System models:**

Even though there are more appropriate sediment representations, in most current ESMs sediment-  
water exchange of OM and chemical elements is either neglected or treated in a very simplistic way  
(Soetaert et al., 2000; Hülse et al., 2017). Most Earth system Models of Intermediate Complexity  
135 (EMICs) and also some of the higher resolution global carbon cycle models represent the sediment-  
water interface either as a reflective or a conservative/semi-reflective boundary (Hülse et al., 2017).  
Thus, all particulate material deposited on the seafloor is either instantaneously consumed (reflec-  
tive boundary), or a fixed fraction is buried in the sediments (conservative/semi-reflective boundary).  
Both highly simplified approaches furthermore completely neglect the exchange of solute species  
140 through the sediment-water interface and, therefore, cannot resolve the complex benthic-pelagic  
coupling. However, due to their computational efficiency, both representations are often used in

global biogeochemical models (e.g. Najjar et al., 2007; Ridgwell et al., 2007; Goosse et al., 2010). A superior approach is the vertically integrated dynamic model, which represents the whole sediment column as a single box (Hülse et al., 2017). Here, OM deposited on the seafloor is added to the sediment box where it gets degraded and dissolved species diffuse through the sediment-water interface in accordance with these transformations. This approach thus ignores the vertical extent of the sediments and the temporary storage of dissolved species (Soetaert et al., 2000). Yet, it is computationally efficient and allows differentiating between various fractions of organic matter. Most EMICs incorporate a vertically integrated dynamic model for particulate inorganic carbon only (i.e. mainly  $\text{CaCO}_3$ ) and just a few consider oxic-only sediment degradation of organic matter (Hülse et al., 2017).

The most complex description of diagenetic organic matter degradation in Earth system models is the second group of vertically resolved diagenetic models as discussed above (e.g. Heinze et al., 1999; Munhoven, 2007; Shaffer et al., 2008). These models solve the one-dimensional reaction-transport equation for a number of solid and dissolved species for the upper, bioturbated 10 cm of the sediments. Examples of global ESMs employing a vertically resolved diagenetic model are NorESM (Tjiputra et al., 2013) and HAMOCC (Palastanga et al., 2011; Ilyina et al., 2013), both using a version of Heinze et al. (1999). None of the EMICs reviewed by Hülse et al. (2017) use such a sediment representation. DCESS (Shaffer et al., 2008) and MBM (Munhoven, 2007) are box models employing a vertically resolved diagenetic model. However, in general oxygen is the only TEA explicitly modelled and secondary redox reactions and reduced species are completely neglected in these approaches. Furthermore, all models represent the bulk OM pool as a single fraction with a fixed degradation rate constant.

#### **Problem with that:**

Obviously, such a simplification of the OM pool can neither account for the observed vast structural complexity in natural organic matter and its resulting different degradation rates nor for the rapid decrease in OM degradability in the uppermost centimetres of the sediments (Arndt et al., 2013). It has been suggested that at least a 3G approach is necessary to accurately represent organic matter dynamics in this part of the sediments where most OM is degraded (e.g. Soetaert et al., 1996b). Even more restrictive is the use of  $\text{O}_2$  as the only TEA and the complete absence of reduced substances and related secondary redox reactions. Even though for the majority of the modern sediments (i.e. in the deep-ocean)  $\text{O}_2$  is the primary electron acceptor and Archer et al. (2002) suggested that aerobic degradation accounts for 66% of total organic matter respiration more recent model and data studies have reported that sulfate reduction is the dominant degradation pathway on a global average (with contributions of 55-76% Canfield et al., 2005; Jørgensen and Kasten, 2006; Thullner et al., 2009).  $\text{O}_2$  becomes progressively less important as TEA with decreasing seafloor depth and in shallow waters most of it is used to reoxidise reduced substances produced during anaerobic degradation (Canfield et al., 2005; Thullner et al., 2009). Thus, the in situ production of e.g.  $\text{NO}_3$  and  $\text{SO}_4$

through oxidation of  $\text{NH}_4$  and  $\text{H}_2\text{S}$  forms an important sink for  $\text{O}_2$  which is entirely neglected in  
 180 current sediment representations in global models. In addition, due to the lack of an appropriate  
 sedimentary P cycle (with the exception of the HAMOCC version of Palastanga et al. (2011), no  
 current global ESM is able to model the redox dependent P release from marine sediments and its  
 implications for primary productivity, global biogeochemical cycles and climate.

#### **Solution presented here:**

185 In order to provide a more realistic description of organic matter degradation and nutrient cycles  
 in marine sediments we have developed the OrganicMatter ENabled SEDiment model (OMEN-  
 SED), a new, one-dimensional, numerically efficient reactive transport model. OMEN-SED is the  
 first analytical model to explicitly describe OM cycling as well as the associated dynamics of the  
 most important TEAs (i.e.  $\text{O}_2$ ,  $\text{NO}_3$ ,  $\text{SO}_4$ ), related reduced substances ( $\text{NH}_4$ ,  $\text{H}_2\text{S}$ ), the full suite  
 190 of secondary-redox reactions, macronutrients ( $\text{PO}_4$ ) and associated pore water quantities (ALK,  
 DIC). To represent a redox-dependent sedimentary P cycle we consider the formation and burial  
 of Fe-bound P and authigenic Ca-P minerals. Thus, OMEN-SED captures most of the features of  
 a complex, numerical diagenetic model, however, its computational efficiency allows the coupling  
 to global Earth System Models and therefore the investigation of coupled global biogeochemical  
 195 dynamics over geological timescales. Here, the model is presented as a 2G-approach, however, a  
 third, non-degradable OM pool can be added and OMEN-SED can easily be extended to a Multi-G  
 approach.

## **2 Model Description**

The following section provides a detailed description of the new model. Table 1 summarizes the  
 200 biogeochemical reaction network and a glossary of parameters along with their respective units is  
 provided in Tables 9 and 10.

### **2.1 General Model Approach**

The calculation of benthic return/uptake and burial fluxes is based on the vertically resolved con-  
 servation equation for solid and dissolved species in porous media (e.g. Berner, 1980; Boudreau,  
 205 1997):

$$\frac{\partial \xi C_i}{\partial t} = -\frac{\partial F}{\partial z} + \xi \sum_j R_i^j \quad (1)$$

where  $C_i$  is the concentration of the biogeochemical species  $i$ ,  $\xi$  equals the porosity  $\phi$  for solute  
 species and  $(1 - \phi)$  for solid species, hence represents the partitioning of species  $i$  into the solute and  
 210 dissolved phase. The term  $z$  is the sediment depth,  $t$  denotes the time,  $F$  summarises the transport  
 fluxes and  $\sum_j R_i^j$  represents the sum of production/consumption rates  $j$  that affect species  $i$ . The re-

action network accounts for the most important primary and secondary redox reactions, equilibrium reactions, mineral dissolution and precipitation, as well as adsorption and desorption processes that affect the explicitly resolved chemical species.

215 State-of-the-art reaction-transport models generally solve the ordinary differential equation (ODE, Eq. 1) numerically and thus allow to account for transient dynamics, depth-varying parameters or a high degree of coupling between different chemical species (e.g. Soetaert et al., 1996b; Aguilera et al., 2005). Yet, numerical models are computational expensive, thus rendering their application in an Earth System Model framework prohibitive. An analytical solution of equation (1) provides an  
220 alternative and computational more efficient approach which enjoyed great popularity in the early days of diagenetic modelling and computer technology. However, early analytical models were often very problem-specific and only considered one or two coupled species (e.g. Berner, 1964). (e.g. Lehrman, Berner) ?? which other pub? Over the next decades, a number of more complex analytical models describing the coupled dynamics of OM degradation, TEAs and reduced substances in sediments were developed (e.g. Billen, 1982; Goloway and Bender, 1982; Jahnke et al., 1982), before  
225 the boost in computing power enabled the development of fully-coupled, multi-species, numerical models (e.g. Van Cappellen and Wang, 1995; Soetaert et al., 1996b).

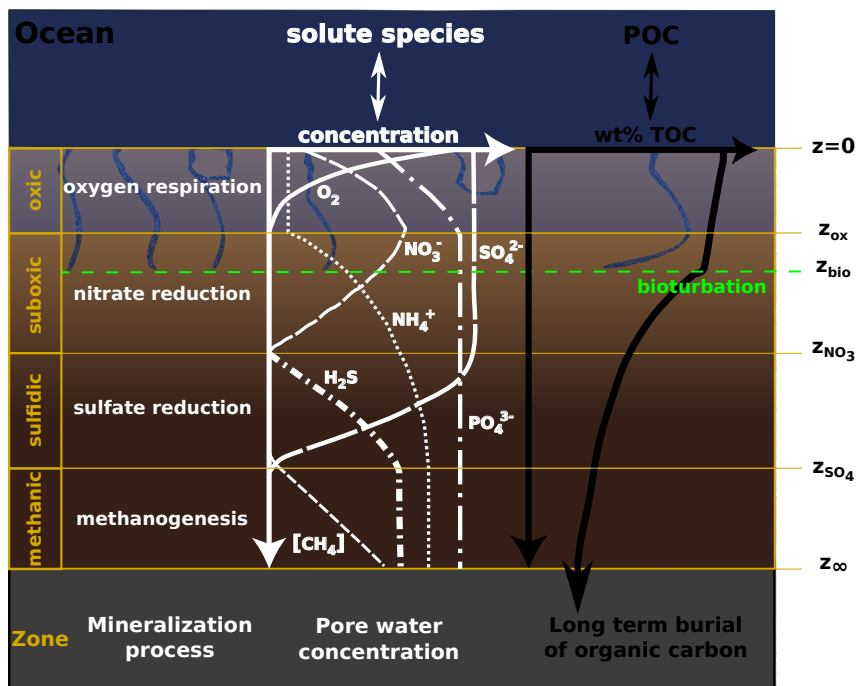


**Figure 1.** Schematic of the different modelled species and layers in OMEN-SED. Here showing the case  $z_{ox} < z_{bio} < z_{NO_3} < z_{SO_4}$ .



Finding an analytical solution to Eq. (1), especially when complex reaction networks are to be considered, is not straightforward and generally requires the assumption of steady state. In addition, the complexity of the reaction network can be reduced by dividing the sediment into distinct zones and accounting for the most pertinent biogeochemical processes within each zone, thus increasing the likelihood of finding an analytical solution to Eq. (1) (see Eq. (30) in section 2.5.1 for the general steady-state solution).

Therefore, OMEN-SED assumes that benthic dynamics can be represented by a series of steady-states. Because the Earth system model relevant variability in boundary conditions and fluxes is generally longer than the characteristic timescales of the reaction-transport processes, the sediment can be described by a series of pseudo steady-states. In addition, it divides the sediment into a bioturbated and a non-bioturbated zone defined by the constant bioturbation depth  $z_{\text{bio}}$  (see Fig. 1). Furthermore, it accounts for the dynamic redox zonation of marine sediments by dividing the sediment into: 2) an oxic zone delineated by the oxygen penetration depth  $z_{\text{ox}}$ , 3) a denitrification zone situated between  $z_{\text{ox}}$  and the nitrate penetration depth  $z_{\text{NO}_3}$ , 4) a sulfate reduction zone situated between  $z_{\text{NO}_3}$  and the sulfate penetration depth  $z_{\text{SO}_4}$  and 5) a methanogenic zone situated below  $z_{\text{SO}_4}$  (Fig. 1). All penetration depths are dynamically calculated by the model. Each zone is characterised by a set of diagenetic equations that encapsulate the most pertinent reaction and transport processes in this zone (see section 2.2 and 2.3 for more details).

OMEN calculates and feeds back to the Earth System model the fraction of POC preserved in the sediments and the sediment-water interface fluxes of the dissolved species  $C_i$  (in  $\text{mol cm}^{-2} \text{ year}^{-1}$ ):

$$\text{Flux\_SWI}(C_i) = \phi \left( D_i \frac{\partial C_i(z)}{\partial z} \Big|_0 - w [C_i(0) - C_i(z_\infty)] \right) \quad (2)$$

where  $w$  is the deposition rate,  $D_i$  is the diffusion coefficient and  $C_i(0)$ ,  $C_i(z_\infty)$  the concentration of species  $i$  at the SWI and at the lower sediment boundary.

## 2.2 Transport

The model accounts for both the advective, as well as the diffusive transport of dissolved and solid species, assuming that sediment compaction is negligible (i.e.  $\frac{\partial \phi}{\partial z} = 0$ ). The molecular diffusion of dissolved species is described via a species-specific apparent diffusion coefficient,  $D_{\text{mol},i}$ . In addition, the activity of infaunal organisms in the bioturbated zone of the sediment ( $z < z_{\text{bio}}$ ) that causes random displacements of sediments and porewaters is simulated using a diffusive term (e.g. Boudreau, 1986), with a constant bioturbation coefficient  $D_{\text{bio}}$  in the bioturbated zone. The pumping activity by burrow-dwelling animals and the resulting ventilation of tubes, the so-called bioirrigation, is encapsulated in a factor,  $f_{ir}$ , that enhances the molecular diffusion coefficient (hence,  $D_{i,0} = D_{\text{mol},i} \cdot f_{ir}$ , Soetaert et al., 1996a). The flux divergence can thus be formulated as:

$$\frac{\partial F}{\partial z} = - \frac{\partial}{\partial z} \left( -\xi D_i \frac{\partial C_i}{\partial z} + \xi w C_i \right) \quad (3)$$

**Table 1.** Reactions and biogeochemical tracers implemented in the Reaction Network of OMEN-SED. The primary and secondary redox reactions are listed in the sequence they occur with increasing sediment depth.

	Description
Primary redox reactions	Degradation of organic matter via aerobic degradation, denitrification, sulfate reduction, methanogenesis (implicit)
Secondary redox reactions	Oxidation of ammonium and sulfide by oxygen, anaerobic oxidation of methane by sulfate
Adsorption/Desorption	Ad-/Desorption of P on/from $\text{Fe}(\text{OH})_3$ , $\text{NH}_4$ adsorption, $\text{PO}_4$ adsorption
Mineral precipitation	Formation of authigenic P
Biogeochemical tracers	Organic matter, oxygen, nitrate, ammonium, sulfate, sulfide (hydrogen sulfide), phosphate, Fe-bound P, DIC, ALK

where  $D_i$  is the diffusion coefficient of species  $i$  ( $D_i = D_{i,0} + D_{\text{bio}} = D_{\text{mol},i} \cdot f_{ir} + D_{\text{bio}}$  for dissolved species and  $D_i = D_{\text{bio}}$  for solid species) and  $w$  is the deposition rate. The bioturbation coefficient  $D_{\text{bio}}$  is set to zero below  $z_{\text{bio}}$ .

## 2.3 Reaction Network

Earth System models generally track the biogeochemical dynamics of organic and inorganic carbon, essential nutrients (nitrogen, phosphorus) and oxygen with the aim of investigating the evolution of the ocean's redox structure and carbonate system and its feedbacks on global climate. This general aim thus defines a minimum set of state variables and reaction processes that need to be resolved for an efficient representation of the benthic-pelagic coupling in Earth system models. A suitable sediment model must provide a robust quantification of organic (and inorganic) carbon burial fluxes, as well as the benthic return fluxes of growth-limiting nutrients, equilibrium invariant and reduced species, and oxygen uptake fluxes. As a consequence, the reaction network must account for the most important primary and secondary redox reactions, equilibrium reactions, mineral precipitation/dissolution and adsorption/desorption, resulting in a complex set of coupled reaction-transport equations. The following subsections provide a short discussion of the reaction processes included in the model and give an overview of the vertically resolved conservation equations and boundary conditions for solid and dissolved species in each layer. Table 1 provides a summary of the reactions and biogeochemical tracers considered in the reaction network. Table 15 summarises their reaction stoichiometry and Table ?? provides an overview of their description in the model.

### 2.3.1 Organic matter or Particulate Organic Carbon (POC)

In marine sediments, organic matter (OM) is degraded by heterotrophic activity coupled to the sequential utilisation of terminal electron acceptors, typically in the order of  $\text{O}_2$ ,  $\text{NO}_3^-$ ,  $\text{Mn}(\text{VI})$ ,  $\text{Fe}(\text{III})$  and  $\text{SO}_4^{2-}$  followed by methanogenesis and/or fermentation. Here, organic matter degra-

**Table 2.** Boundary conditions for organic matter. For the boundaries we define:  $z_{\text{bio}}^- := \lim_{h \rightarrow 0} (z_{\text{bio}} - h)$  and  $z_{\text{bio}}^+ := \lim_{h \rightarrow 0} (z_{\text{bio}} + h)$ .

Boundary	Condition	
$z = 0$	known concentration	1) $C_i(0) = C_{i0}$
$z = z_{\text{bio}}$	continuity	2) $C_i(z_{\text{bio}}^-) = C_i(z_{\text{bio}}^+)$
		3) $-D_{\text{bio}} \cdot \frac{\partial C_i}{\partial z} \Big _{z_{\text{bio}}^-} = 0$

dation is described via a multi-G model approach (Arndt et al., 2013, and references therein), assuming that the bulk OM consists of a number of discrete compound classes  $C_i$  characterised by specific degradation rate constants  $k_i$ . Such a multi-G approach allows for selective preservation of compound classes according to their reactivity,  $k_i$  and, thus, accounts for the change in organic matter reactivity during burial. Each compound class is degraded according to first-order kinetics. The conservation equation for organic matter dynamics is thus given by:

$$\frac{\partial C_i}{\partial t} = 0 = D_{C_i} \frac{\partial^2 C_i}{\partial z^2} - w \frac{\partial C_i}{\partial z} - k_i \cdot C_i \quad (4)$$

The analytical solution of Eq. (4) (see section 2.5 for details) requires the definition of a set of boundary conditions (Table 2). The model assumes a known concentration/flux at the sediment-water interface and continuity across the bottom of the bioturbated zone,  $z_{\text{bio}}$ .

### 2.3.2 Oxygen

In marine sediments, oxygen is consumed via aerobic degradation of organic matter and a number of secondary redox reactions. In the oxic layer ( $z < z_{\text{ox}}$ ), the model explicitly accounts for the aerobic degradation of OM, which consumes oxygen with a fixed  $\text{O}_2 : \text{C}$  ratio ( $\text{O}_2\text{C}$ , Tab. 10) and produces ammonium, which is partially nitrified to nitrate ( $\gamma_{\text{NH}_4}$ ). In addition, the oxygen consumption due to oxidation of reduced species ( $\text{NH}_4$ ,  $\text{H}_2\text{S}$ ) produced in the suboxic and anoxic layers of the sediment is implicitly taken into account through the flux boundary condition at the dynamic oxygen penetration depth  $z_{\text{ox}}$ . This simplification can be justified as it has been shown that these secondary redox reactions mainly occur at the oxic/suboxic interface (Soetaert et al., 1996b). The factor  $\frac{1-\phi}{\phi}$  accounts for the volume conversion from the solid to the dissolved phase. Oxygen dynamics are thus described by:

$$\frac{\partial \text{O}_2}{\partial t} = 0 = D_{\text{O}_2} \frac{\partial^2 \text{O}_2}{\partial z^2} - w \frac{\partial \text{O}_2}{\partial z} - \frac{1-\phi}{\phi} \sum_i k_i \cdot [\text{O}_2\text{C} + 2\gamma_{\text{NH}_4} \text{NC}_i] \cdot C_i(z) \quad (5)$$

The analytical solution of Eq. (5) requires the definition of boundary conditions (Table 3). OMEN-SED assumes a known bottom water concentration and the complete consumption of oxygen at the oxygen penetration depth (or zero flux if  $z_{\text{ox}} = z_{\infty}$ ). Equal oxygen concentration and diffusive

**Table 3.** Boundary conditions for oxygen. For the boundaries we define:  $z_{\text{bio}}^- := \lim_{h \rightarrow 0} (z_{\text{bio}} - h)$  and  $z_{\text{bio}}^+ := \lim_{h \rightarrow 0} (z_{\text{bio}} + h)$ .

Boundary	Condition	
$z = 0$	known concentration	1) $O_2(0) = O_{20}$
$z = z_{\text{bio}}$	continuity	2) $O_2(z_{\text{bio}}^-) = O_2(z_{\text{bio}}^+)$
		3) $-(D_{O_2,0} + D_{\text{bio}}) \cdot \frac{\partial O_2}{\partial z} \Big _{z_{\text{bio}}^-} = -D_{O_2,0} \cdot \frac{\partial O_2}{\partial z} \Big _{z_{\text{bio}}^+}$
$z = z_{\text{ox}}$	$O_2$ consumption ( $z_{\text{ox}} = z_{\infty}$ )	4) <b>IF</b> ( $O_2(z_{\infty}) > 0$ ) $\frac{\partial O_2}{\partial z} \Big _{z_{\text{ox}}} = 0$
	( $z_{\text{ox}} < z_{\infty}$ ) with flux from below	<b>ELSE</b> $O_2(z_{\text{ox}}) = 0$ and $-D_{O_2} \cdot \frac{\partial O_2}{\partial z} \Big _{z_{\text{ox}}} = F_{\text{red}}(z_{\text{ox}})$ $F_{\text{red}}(z_{\text{ox}}) = \frac{1-\phi}{\phi} \cdot \int_{z_{\text{ox}}}^{\infty} \sum_i (2\gamma_{\text{NH}_4} \text{NC}_i + 2\gamma_{\text{H}_2\text{S}} \text{SO}_4\text{C}) k_i C_i dz$

flux above ( $z_{\text{bio}}^-$ ) and below ( $z_{\text{bio}}^+$ ) the bioturbation boundary is considered. In addition, the model accounts for reduced species produced by anaerobic mineralization diffusing into the oxic layer from below, assuming that respective fractions ( $\gamma_{\text{NH}_4}$  and  $\gamma_{\text{H}_2\text{S}}$ ) are re-oxidised at the oxic/suboxic interface.

### 2.3.3 Nitrate and Ammonium

To model nitrate and ammonium dynamics the sediment is partitioned into two geochemical layers (oxic and suboxic), where different equations describe the biogeochemical processes. Above the oxygen penetration depth organic matter mineralization produces ammonium, which is partly nitrified to nitrate (the fraction  $\gamma_{\text{NH}_4}$ ). In the suboxic zone ( $z > z_{\text{ox}}$ ), oxygen concentration is zero and nitrate serves as the electron acceptor to respire organic matter, thus nitrate is consumed by denitrification and ammonium is produced. Below the nitrate penetration depth  $z_{\text{NO}_3}$ , ammonium is still produced via OM mineralization. The model assumes that adsorption of ammonium to sediment particles is fast compared with the characteristic transport time scales. Thus, a constant equilibrium adsorption coefficient  $K_{\text{NH}_4}$  is used to parameterize the loss of dissolved  $\text{NH}_4$  to adsorbed  $\text{NH}_4$  (Wang and Van Cappellen, 1996). Therefore the diagenetic equations for nitrate and ammonium are given by:

1. Layer ( $z \leq z_{\text{ox}}$ )

$$\frac{\partial \text{NO}_3^I}{\partial t} = 0 = D_{\text{NO}_3} \frac{\partial^2 \text{NO}_3^I}{\partial z^2} - w \frac{\partial \text{NO}_3^I}{\partial z} + \gamma_{\text{NH}_4} \frac{1-\phi}{\phi} \cdot \sum_i \text{NC}_i \cdot k_i \cdot C_i(z) \quad (6)$$

$$\frac{\partial \text{NH}_4^I}{\partial t} = 0 = \frac{D_{\text{NH}_4}}{1 + K_{\text{NH}_4}} \frac{\partial^2 \text{NH}_4^I}{\partial z^2} - w \frac{\partial \text{NH}_4^I}{\partial z} + \frac{1 - \gamma_{\text{NH}_4}}{1 + K_{\text{NH}_4}} \cdot \frac{1-\phi}{\phi} \cdot \sum_i \text{NC}_i \cdot k_i \cdot C_i(z) \quad (7)$$

2. Layer ( $z_{\text{ox}} < z \leq z_{\text{NO}_3}$ )

$$\frac{\partial \text{NO}_3^{II}}{\partial t} = 0 = D_{\text{NO}_3} \frac{\partial^2 \text{NO}_3^{II}}{\partial z^2} - w \frac{\partial \text{NO}_3^{II}}{\partial z} - \frac{1-\phi}{\phi} \text{NO}_3 \text{C} \cdot \sum_i k_i \cdot C_i(z) \quad (8)$$

$$\frac{\partial \text{NH}_4^{II}}{\partial t} = 0 = \frac{D_{\text{NH}_4}}{1 + K_{\text{NH}_4}} \frac{\partial^2 \text{NH}_4^{II}}{\partial z^2} - w \frac{\partial \text{NH}_4^{II}}{\partial z} \quad (9)$$

3. Layer ( $z_{\text{NO}_3} < z \leq z_{\infty}$ )

$$\frac{\partial \text{NH}_4^{III}}{\partial t} = 0 = \frac{D_{\text{NH}_4}}{1 + K_{\text{NH}_4}} \frac{\partial^2 \text{NH}_4^{III}}{\partial z^2} - w \frac{\partial \text{NH}_4^{III}}{\partial z} + \frac{1}{1 + K_{\text{NH}_4}} \cdot \frac{1-\phi}{\phi} \cdot \sum_i \text{NC}_i \cdot k_i \cdot C_i(z) \quad (10)$$

The boundary conditions to solve Equations 6 - 10 are summarized in Table 4. The model assumes known bottom water concentrations for both species, the complete consumption of nitrate at the nitrate penetration depth (or zero flux if  $z_{\text{NO}_3} = z_{\infty}$ ) and no change in ammonium flux at  $z_{\infty}$ . It considers equal concentrations and diffusive fluxes at  $z_{\text{bio}}$  and  $z_{\text{ox}}$ . In addition, the re-oxidation of upward-diffusing reduced ammonium is considered in the oxic-suboxic boundary condition for nitrate and ammonium.

### 2.3.4 Sulfate and Sulfide

When nitrate is depleted, sulfate reduction is the pathway to mineralize organic matter, thus consuming sulfate ( $\text{SO}_4$ ) and producing hydrogen sulfide ( $\text{H}_2\text{S}$ ) until the sulfate penetration depth ( $z_{\text{SO}_4}$ ).

Sulfate and sulfide dynamics are thus described by:

1. Layer ( $z \leq z_{\text{NO}_3}$ )

$$\frac{\partial \text{SO}_4^I}{\partial t} = 0 = D_{\text{SO}_4} \frac{\partial^2 \text{SO}_4^I}{\partial z^2} - w \frac{\partial \text{SO}_4^I}{\partial z} \quad (11)$$

$$\frac{\partial \text{H}_2\text{S}^I}{\partial t} = 0 = D_{\text{H}_2\text{S}} \frac{\partial^2 \text{H}_2\text{S}^I}{\partial z^2} - w \frac{\partial \text{H}_2\text{S}^I}{\partial z} \quad (12)$$

2. Layer ( $z_{\text{NO}_3} < z \leq z_{\text{SO}_4}$ )

$$\frac{\partial \text{SO}_4^{II}}{\partial t} = 0 = D_{\text{SO}_4} \frac{\partial^2 \text{SO}_4^{II}}{\partial z^2} - w \frac{\partial \text{SO}_4^{II}}{\partial z} - \frac{1-\phi}{\phi} \cdot \sum_i \text{SO}_4 \text{C} \cdot k_i \cdot C_i(z) \quad (13)$$

$$\frac{\partial \text{H}_2\text{S}^{II}}{\partial t} = 0 = D_{\text{H}_2\text{S}} \frac{\partial^2 \text{H}_2\text{S}^{II}}{\partial z^2} - w \frac{\partial \text{H}_2\text{S}^{II}}{\partial z} + \frac{1-\phi}{\phi} \cdot \sum_i \text{SO}_4 \text{C} \cdot k_i \cdot C_i(z) \quad (14)$$

3. Layer ( $z_{\text{SO}_4} < z \leq z_{\infty}$ )

$$\frac{\partial \text{H}_2\text{S}^{III}}{\partial t} = 0 = D_{\text{H}_2\text{S}} \frac{\partial^2 \text{H}_2\text{S}^{III}}{\partial z^2} - w \frac{\partial \text{H}_2\text{S}^{III}}{\partial z} \quad (15)$$

To solve equations 11 - 15 the model assumes known concentrations at the sediment-water interface and continuity across the bioturbation depth and the nitrate penetration depth (see Table 5).

**Table 4.** Boundary conditions for nitrate and ammonium. For the boundaries we define:  $z_-^- := \lim_{h \rightarrow 0} (z_- - h)$  and  $z_-^+ := \lim_{h \rightarrow 0} (z_- + h)$ .

Boundary	Condition	
$z = 0$	known concentration	1) $NO_3(0) = NO_{30}$
$z = z_{\text{bio}}$	continuity	2) $NO_3(z_{\text{bio}}^-) = NO_3(z_{\text{bio}}^+)$
		3) $-(D_{NO_3,0} + D_{\text{bio}}) \cdot \frac{\partial NO_3}{\partial z} \Big _{z_{\text{bio}}^-} = -D_{NO_3,0} \cdot \frac{\partial NO_3}{\partial z} \Big _{z_{\text{bio}}^+}$
$z = z_{\text{ox}}$	continuity	4) $NO_3(z_{\text{ox}}^-) = NO_3(z_{\text{ox}}^+)$
	where:	5) $-D_{NO_3} \cdot \frac{\partial NO_3}{\partial z} \Big _{z_{\text{ox}}^-} + \gamma_{\text{NH}_4} \cdot F_{\text{NH}_4}(z_{\text{ox}}) = -D_{NO_3} \cdot \frac{\partial NO_3}{\partial z} \Big _{z_{\text{ox}}^+}$
$z = z_{\text{NO}_3}$	NO <sub>3</sub> consumption ( $z_{\text{NO}_3} = z_{\infty}$ )	$F_{\text{NH}_4}(z_{\text{ox}}) = \frac{1}{1+K_{\text{NH}_4}} \cdot \frac{1-\phi}{\phi} \cdot \int_{z_{\text{NO}_3}}^{\infty} \sum_i k_i \cdot \text{NC}_i \cdot C_i dz$
	( $z_{\text{NO}_3} < z_{\infty}$ )	6) <b>IF</b> ( $NO_3(z_{\infty}) > 0$ ) $\frac{\partial NO_3}{\partial z} \Big _{z_{\text{NO}_3}} = 0$ <b>ELSE</b> $NO_3(z_{\text{NO}_3}) = 0$
$z = 0$	known concentration	1) $NH_4(0) = NH_{40}$
$z = z_{\text{bio}}$	continuity	2) $NH_4(z_{\text{bio}}^-) = NH_4(z_{\text{bio}}^+)$
		3) $-\frac{D_{\text{NH}_4,0} + D_{\text{bio}}}{1+K_{\text{NH}_4}} \cdot \frac{\partial NH_4}{\partial z} \Big _{z_{\text{bio}}^-} = -\frac{D_{\text{NH}_4,0}}{1+K_{\text{NH}_4}} \cdot \frac{\partial NH_4}{\partial z} \Big _{z_{\text{bio}}^+}$
$z = z_{\text{ox}}$	continuity	4) $NH_4(z_{\text{ox}}^-) = NH_4(z_{\text{ox}}^+)$
	where:	5) $-\frac{D_{\text{NH}_4}}{1+K_{\text{NH}_4}} \cdot \frac{\partial NH_4}{\partial z} \Big _{z_{\text{ox}}^-} - \gamma_{\text{NH}_4} \cdot F_{\text{NH}_4}(z_{\text{ox}}) = -\frac{D_{\text{NH}_4}}{1+K_{\text{NH}_4}} \cdot \frac{\partial NH_4}{\partial z} \Big _{z_{\text{ox}}^+}$
$z = z_{\text{NO}_3}$	continuity	$F_{\text{NH}_4}(z_{\text{ox}}) = \frac{1}{1+K_{\text{NH}_4}} \cdot \frac{1-\phi}{\phi} \cdot \int_{z_{\text{NO}_3}}^{\infty} \sum_i k_i \cdot \text{NC}_i \cdot C_i dz$
	flux	6) $NH_4(z_{\text{NO}_3}^-) = NH_4(z_{\text{NO}_3}^+)$
$z = z_{\infty}$	zero NH <sub>4</sub> flux	7) $-\frac{D_{\text{NH}_4}}{1+K_{\text{NH}_4}} \cdot \frac{\partial NH_4}{\partial z} \Big _{z_{\text{NO}_3}^-} = -\frac{D_{\text{NH}_4}}{1+K_{\text{NH}_4}} \cdot \frac{\partial NH_4}{\partial z} \Big _{z_{\text{NO}_3}^+}$ 8) $\frac{\partial NH_4}{\partial z} \Big _{z_{\infty}} = 0$

365 The re-oxidation of reduced H<sub>2</sub>S to SO<sub>4</sub> is considered in the oxic-suboxic boundary condition for both species, here including the methanic zone, as H<sub>2</sub>S is also produced during anaerobic oxidation of methane (AOM). Furthermore, sulfate is used at  $z_{\text{SO}_4}$  to oxidize methane from below and thus producing H<sub>2</sub>S. In case  $z_{\text{SO}_4} < z_{\infty}$ , sulfate concentration is zero at  $z_{\text{SO}_4}$  and its diffusive flux must equal the amount of methane produced below; or, in case  $z_{\text{SO}_4} = z_{\infty}$ , a zero flux condition for sulfate is considered. At the lower boundary  $z_{\infty}$  zero flux of H<sub>2</sub>S is considered. **correct??**

370

### 2.3.5 Phosphate

To model phosphorus (P) dynamics in the sediments OMEN-SED takes into account the change with depth of phosphate (PO<sub>4</sub>) and iron-bound P, thereby mainly following the description of Slomp et al. (1996) and Gypens et al. (2008). Throughout the sediment column organic matter is mineralized resulting in a release of phosphate to the pore water. In the oxic part of the sediment, this PO<sub>4</sub> either diffuses upward to the water column or is adsorbed to Fe oxides forming Fe-bound P (or M) (Slomp

375

**Table 5.** Boundary conditions for sulfate and sulfide. For the boundaries we define:  $z_-^- := \lim_{h \rightarrow 0} (z_- - h)$  and  $z_-^+ := \lim_{h \rightarrow 0} (z_- + h)$ .

Boundary	Condition	
$z = 0$	known concentration	1) $\text{SO}_4(0) = \text{SO}_{40}$
$z = z_{\text{bio}}$	continuity	2) $\text{SO}_4(z_{\text{bio}}^-) = \text{SO}_4(z_{\text{bio}}^+)$
	flux	3) $-(D_{\text{SO}_4,0} + D_{\text{bio}}) \cdot \frac{\partial \text{SO}_4}{\partial z} \Big _{z_{\text{bio}}^-} = -D_{\text{SO}_4,0} \cdot \frac{\partial \text{SO}_4}{\partial z} \Big _{z_{\text{bio}}^+}$ <b>DH: @Sandra: BC 5)</b>
$z = z_{\text{ox}}$	continuity	4) $\text{SO}_4(z_{\text{ox}}^-) = \text{SO}_4(z_{\text{ox}}^+)$ <b>Include <math>\int_{z_{\text{SO}_4}}^\infty</math> here?</b>
	flux	5) $-D_{\text{SO}_4} \cdot \frac{\partial \text{SO}_4}{\partial z} \Big _{z_{\text{ox}}^-} + \gamma_{\text{H}_2\text{S}} \cdot F_{\text{H}_2\text{S}}(z_{\text{ox}}) = -D_{\text{SO}_4} \cdot \frac{\partial \text{SO}_4}{\partial z} \Big _{z_{\text{ox}}^+}$
	where:	$F_{\text{H}_2\text{S}}(z_{\text{ox}}) = \frac{1-\phi}{\phi} \cdot \left( \int_{z_{\text{NO}_3}}^{\text{SO}_4} \sum_i \text{SO}_4 \text{C} \cdot k_i \cdot C_i \, dz + \gamma_{\text{CH}_4} \cdot \int_{z_{\text{SO}_4}}^\infty \sum_i \text{MC} \cdot k_i \cdot C_i \, dz \right)$
$z = z_{\text{NO}_3}$	continuity	6) $\text{SO}_4(z_{\text{NO}_3}^-) = \text{SO}_4(z_{\text{NO}_3}^+)$
	flux	7) $-D_{\text{SO}_4} \cdot \frac{\partial \text{SO}_4}{\partial z} \Big _{z_{\text{NO}_3}^-} = -D_{\text{SO}_4} \cdot \frac{\partial \text{SO}_4}{\partial z} \Big _{z_{\text{NO}_3}^+}$ <b>DH: @Sandra: think yes,</b>
$z = z_{\text{SO}_4}$	$\text{SO}_4$ consumption	8) <b>IF</b> $(\text{SO}_4(z_\infty) > 0)$ <b>because at 8) <math>\text{CH}_4</math> from</b>
	$(z_{\text{SO}_4} = z_\infty)$	$\frac{\partial \text{SO}_4}{\partial z} \Big _{z_{\text{SO}_4}} = 0$ <b><math>\int_{z_{\text{SO}_4}}^\infty</math> is oxidised to <math>\text{H}_2\text{S}</math>,</b>
	$(z_{\text{SO}_4} < z_\infty)$	<b>ELSE</b> $\text{SO}_4(z_{\text{SO}_4}) = 0$ and $-D_{\text{SO}_4} \cdot \frac{\partial \text{SO}_4}{\partial z} \Big _{z_{\text{SO}_4}} = \gamma_{\text{CH}_4} \cdot F_{\text{CH}_4}(z_{\text{SO}_4})$ <b>at 5) this <math>\text{H}_2\text{S}</math> to <math>\text{SO}_4</math></b>
	with flux from below:	$F_{\text{CH}_4}(z_{\text{SO}_4}) = \frac{1-\phi}{\phi} \cdot \int_{z_{\text{SO}_4}}^\infty \sum_i \text{MC} \cdot k_i \cdot C_i \, dz$
$z = 0$	known concentration	1) $\text{H}_2\text{S}(0) = \text{H}_2\text{S}_0$
$z = z_{\text{bio}}$	continuity	2) $\text{H}_2\text{S}(z_{\text{bio}}^-) = \text{H}_2\text{S}(z_{\text{bio}}^+)$
	flux	3) $-(D_{\text{H}_2\text{S},0} + D_{\text{bio}}) \cdot \frac{\partial \text{H}_2\text{S}}{\partial z} \Big _{z_{\text{bio}}^-} = -D_{\text{H}_2\text{S},0} \cdot \frac{\partial \text{H}_2\text{S}}{\partial z} \Big _{z_{\text{bio}}^+}$
$z = z_{\text{ox}}$	continuity	4) $\text{H}_2\text{S}(z_{\text{ox}}^-) = \text{H}_2\text{S}(z_{\text{ox}}^+)$
	flux	5) $-D_{\text{H}_2\text{S}} \cdot \frac{\partial \text{H}_2\text{S}}{\partial z} \Big _{z_{\text{ox}}^-} - \gamma_{\text{H}_2\text{S}} F_{\text{H}_2\text{S}}(z_{\text{ox}}) = -D_{\text{H}_2\text{S}} \cdot \frac{\partial \text{H}_2\text{S}}{\partial z} \Big _{z_{\text{ox}}^+}$
	where:	$F_{\text{H}_2\text{S}}(z_{\text{ox}}) = \frac{1-\phi}{\phi} \cdot \left( \int_{z_{\text{NO}_3}}^{\text{SO}_4} \sum_i \text{SO}_4 \text{C} \cdot k_i \cdot C_i \, dz + \gamma_{\text{CH}_4} \cdot \int_{z_{\text{SO}_4}}^\infty \sum_i \text{MC} \cdot k_i \cdot C_i \, dz \right)$
$z = z_{\text{NO}_3}$	continuity	6) $\text{H}_2\text{S}(z_{\text{NO}_3}^-) = \text{H}_2\text{S}(z_{\text{NO}_3}^+)$
	flux	7) $-D_{\text{H}_2\text{S}} \cdot \frac{\partial \text{H}_2\text{S}}{\partial z} \Big _{z_{\text{NO}_3}^-} = -D_{\text{H}_2\text{S}} \cdot \frac{\partial \text{H}_2\text{S}}{\partial z} \Big _{z_{\text{NO}_3}^+}$
$z = z_{\text{SO}_4}$	continuity	8) $\text{H}_2\text{S}(z_{\text{SO}_4}^-) = \text{H}_2\text{S}(z_{\text{SO}_4}^+)$
	flux (with AOM)	9) $-D_{\text{H}_2\text{S}} \cdot \frac{\partial \text{H}_2\text{S}}{\partial z} \Big _{z_{\text{SO}_4}^-} + \gamma_{\text{CH}_4} \cdot F_{\text{CH}_4}(z_{\text{SO}_4}) = -D_{\text{H}_2\text{S}} \cdot \frac{\partial \text{H}_2\text{S}}{\partial z} \Big _{z_{\text{SO}_4}^+}$
	where:	$F_{\text{CH}_4}(z_{\text{SO}_4}) = \frac{1-\phi}{\phi} \cdot \int_{z_{\text{SO}_4}}^\infty \sum_i \text{MC} \cdot k_i \cdot C_i \, dz$
$z = z_\infty$	zero $\text{H}_2\text{S}$ flux	10) $\frac{\partial \text{H}_2\text{S}}{\partial z} \Big _{z_\infty} = 0$

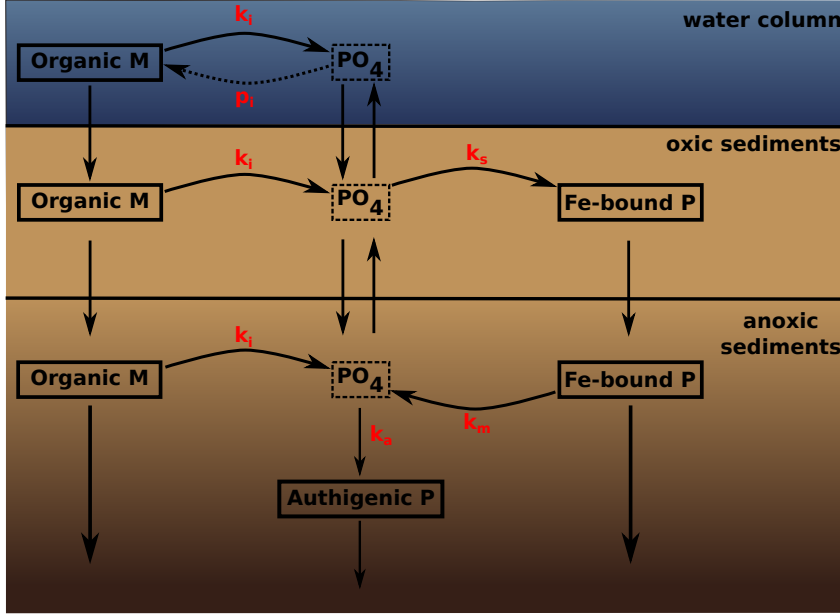


**Figure 2.** A schematic of the sedimentary P cycle in OMEN-SED. Red numbers represent kinetic rate constants for phosphorus dynamics (compare Table 10;  $p_i$  represents uptake rate of  $\text{PO}_4$  via primary production in shallow environments). Adapted from Slomp et al. (1996).

et al., 1998). In the suboxic/anoxic zone,  $\text{PO}_4$  is not only produced via organic matter degradation but is also released from the Fe-bound P pool due to the reduction of Fe oxides. Furthermore, phosphate concentrations can become high enough in this layer for authigenic mineral formation to occur (Van Cappellen and Berner, 1988). This phosphorus bound in authigenic minerals represents a permanent sink for reactive phosphorus (Slomp et al., 1996). See Figure 2 for a schematic overview of the sedimentary P cycle. As for ammonium, the adsorption of P to the sediment matrix is treated as an equilibrium processes, parameterized with dimensionless adsorption coefficients for the oxic and anoxic zone ( $K_{\text{PO}_4}^I$ ,  $K_{\text{PO}_4}^{II}$  Slomp et al., 1998). Therefore the diagenetic equations for phosphate are written as:

1. Layer ( $z \leq z_{\text{ox}}$ )

$$\frac{\partial \text{PO}_4^I}{\partial t} = \frac{D_{\text{PO}_4}}{1 + K_{\text{PO}_4}^I} \frac{\partial^2 \text{PO}_4^I}{\partial z^2} - w \frac{\partial \text{PO}_4^I}{\partial z} + \frac{1 - \phi}{\phi} \frac{1}{1 + K_{\text{PO}_4}^I} \sum_i (\text{PC}_i \cdot k_i \cdot C_i(z)) - \frac{k_s}{1 + K_{\text{PO}_4}^I} (\text{PO}_4^I - \text{PO}_4^s) \quad (16)$$

$$\frac{\partial M^I}{\partial t} = D_M \frac{\partial^2 M^I}{\partial z^2} - w \frac{\partial M^I}{\partial z} + \frac{\phi}{1 - \phi} k_s (\text{PO}_4^I - \text{PO}_4^s) \quad (17)$$



**Table 6.** Boundary conditions for phosphate and Fe-bound P (M). For the boundaries we define:  $z_- := \lim_{h \rightarrow 0} (z_- - h)$  and  $z_+ := \lim_{h \rightarrow 0} (z_- + h)$ .

Boundary	Condition	
$z = 0$	known concentration	1) $\text{PO}_4(0) = \text{PO}_{40}$
$z = z_{\text{bio}}$	continuity	2) $\text{PO}_4(z_{\text{bio}}^-) = \text{PO}_4(z_{\text{bio}}^+)$
	flux	3) $(D_{\text{PO}_4,0} + D_{\text{bio}}) \cdot \frac{\partial \text{PO}_4}{\partial z} \Big _{z_{\text{bio}}^-} = D_{\text{PO}_4,0} \cdot \frac{\partial \text{PO}_4}{\partial z} \Big _{z_{\text{bio}}^+}$
$z = z_{\text{ox}}$	continuity	4) $\text{PO}_4(z_{\text{ox}}^-) = \text{PO}_4(z_{\text{ox}}^+)$
	flux	5) $-\frac{D_{\text{PO}_4}}{1+K_{\text{PO}_4}^{\text{II}}} \cdot \frac{\partial \text{PO}_4}{\partial z} \Big _{z_{\text{ox}}^-} = -\frac{D_{\text{PO}_4}}{1+K_{\text{PO}_4}^{\text{II}}} \cdot \frac{\partial \text{PO}_4}{\partial z} \Big _{z_{\text{ox}}^+}$
$z = z_{\infty}$	flux	10) $\frac{\partial \text{PO}_4}{\partial z} \Big _{z_{\infty}} = 0$
$z = 0$	known concentration	1) $M(0) = M_0$
$z = z_{\text{bio}}$	continuity	2) $M(z_{\text{bio}}^-) = M(z_{\text{bio}}^+)$
	flux	3) $\frac{\partial M}{\partial z} \Big _{z_{\text{bio}}^-} = \frac{\partial M}{\partial z} \Big _{z_{\text{bio}}^+}$
$z = z_{\text{ox}}$	continuity	4) $M(z_{\text{ox}}^-) = M(z_{\text{ox}}^+)$
	flux	5) $\frac{\partial M}{\partial z} \Big _{z_{\text{ox}}^-} = \frac{\partial M}{\partial z} \Big _{z_{\text{ox}}^+}$
$z = z_{\infty}$	asymptotic concentration	10) $M(z_{\infty}) = M_{\infty}$

## 2. Layer ( $z_{\text{ox}} < z$ )

$$\frac{\partial M^{\text{II}}}{\partial t} = D_M \frac{\partial^2 M^{\text{II}}}{\partial z^2} - w \frac{\partial M^{\text{II}}}{\partial z} - k_m (M^{\text{II}} - M^{\infty}) \quad (18)$$

$$\begin{aligned} \frac{\partial \text{PO}_4^{\text{II}}}{\partial t} = & \frac{D_{\text{PO}_4}}{1+K_{\text{PO}_4}^{\text{II}}} \frac{\partial^2 \text{PO}_4^{\text{II}}}{\partial z^2} - w \frac{\partial \text{PO}_4^{\text{II}}}{\partial z} + \frac{1-\phi}{\phi} \frac{1}{1+K_{\text{PO}_4}^{\text{II}}} \sum_i (\text{PC}_i \cdot k_i \cdot C_i(z)) \\ & - \frac{k_a}{1+K_{\text{PO}_4}^{\text{II}}} (\text{PO}_4^{\text{II}} - \text{PO}_4^a) + \frac{(1-\phi)}{\phi} \frac{k_m}{1+K_{\text{PO}_4}^{\text{II}}} (M^{\text{II}} - M^{\infty}) \end{aligned} \quad (19)$$

$$(20)$$

The boundary conditions to solve Equations 16 - 19 are summarized in Table 6. The model assumes known bottom water concentrations and equal concentrations and diffusive fluxes at  $z_{\text{bio}}$  and  $z_{\text{ox}}$  for both species. Additionally it considers no change in phosphate flux and an asymptotic Fe-bound P concentration at  $z_{\infty}$ .

### 2.3.6 Dissolved Inorganic Carbon (DIC)

Organic matter degradation produces dissolved inorganic carbon (DIC) with a stoichiometric DIC:C ratio of 1:2 in the methanic zone and 1:1 in the rest of the sediment column. DIC dynamics in OMEN-SED are thus described by equations 21 and 21 and boundary conditions as summarized in Table 7. The model assumes a known DIC concentration at the sediment-water interface, a zero flux condition at the lower boundary  $z_{\infty}$  and continuity across the bioturbation and sulfate penetration depth. In

**Table 7.** Boundary conditions for DIC. For the boundaries we define:  $z_-^- := \lim_{h \rightarrow 0} (z_- - h)$  and  $z_-^+ := \lim_{h \rightarrow 0} (z_- + h)$ .

Boundary	Condition	
$z = 0$	known concentration	1) $DIC(0) = DIC_0$
$z = z_{\text{bio}}$	continuity	2) $DIC(z_{\text{bio}}^-) = DIC(z_{\text{bio}}^+)$
	flux	3) $-(D_{DIC,0} + D_{\text{bio}}) \cdot \frac{\partial DIC}{\partial z} \Big _{z_{\text{bio}}^-} = -D_{DIC,0} \cdot \frac{\partial DIC}{\partial z} \Big _{z_{\text{bio}}^+}$
$z = z_{\text{SO}_4}$	continuity	4) $DIC(z_{\text{SO}_4}^-) = DIC(z_{\text{SO}_4}^+)$
	flux (with AOM)	5) $-D_{DIC} \cdot \frac{\partial DIC}{\partial z} \Big _{z_{\text{SO}_4}^-} + \gamma_{\text{CH}_4} \cdot F_{\text{CH}_4}(z_{\text{SO}_4}) = -D_{DIC} \cdot \frac{\partial DIC}{\partial z} \Big _{z_{\text{SO}_4}^+}$
	where:	$F_{\text{CH}_4}(z_{\text{SO}_4}) = \frac{1-\phi}{\phi} \cdot \int_{z_{\text{SO}_4}}^{\infty} \sum_i MC \cdot k_i \cdot C_i dz$
$z = z_{\infty}$	zero DIC flux	6) $\frac{\partial DIC}{\partial z} \Big _{z_{\infty}} = 0$

410 addition, the anaerobic oxidation of methane at  $z_{\text{SO}_4}$  produces DIC (with 1:1 stoichiometry) which is accounted for through the flux boundary condition at  $z_{\text{SO}_4}$  (Table 7 eq. 5)

1. Layer ( $z \leq z_{\text{SO}_4}$ )

415 
$$\frac{\partial DIC^I}{\partial t} = 0 = D_{DIC} \frac{\partial^2 DIC^I}{\partial z^2} - w \frac{\partial DIC^I}{\partial z} + \frac{1-\phi}{\phi} \cdot \sum_i DIC^I \cdot k_i \cdot C_i(z) \quad (21)$$

2. Layer ( $z_{\text{SO}_4} < z \leq z_{\infty}$ )

$$\frac{\partial DIC^{II}}{\partial t} = 0 = D_{DIC} \frac{\partial^2 DIC^{II}}{\partial z^2} - w \frac{\partial DIC^{II}}{\partial z} + \frac{1-\phi}{\phi} \cdot \sum_i DIC^{II} \cdot k_i \cdot C_i(z) \quad (22)$$

### 420 2.3.7 Alkalinity

Organic matter degradation and secondary redox reactions exert a complex influence on alkalinity with opposite effects depending on the TEA involved (Wolf-Gladrow et al., 2007). To model alkalinity in OMEN-SED the sediment column is partitioned into four geochemical layers, where different equations describe the biogeochemical processes using variable stoichiometric coefficients (compare Tables 10 and 15). Above  $z_{\text{ox}}$ , the combined effects of  $\text{NH}_4$  and P release due to aerobic OM mineralization increases alkalinity according to  $\text{ALK}^{\text{OX}}$  whereas nitrification decreases alkalinity with stoichiometry  $\text{ALK}^{\text{NIT}}$ . In the remaining three zones anaerobic OM mineralization increases alkalinity with variable stoichiometric coefficients (i.e.  $\text{ALK}^{\text{DEN}}$ ,  $\text{ALK}^{\text{SUL}}$ ,  $\text{ALK}^{\text{MET}}$ ). Thus, the diagenetic equations for alkalinity are written as:

430

1. Layer ( $z \leq z_{\text{ox}}$ )

$$\begin{aligned} \frac{\partial \text{ALK}^I}{\partial t} = 0 = D_{\text{ALK}} \frac{\partial^2 \text{ALK}^I}{\partial z^2} - w \frac{\partial \text{ALK}^I}{\partial z} \\ + \frac{1-\phi}{\phi} \cdot \sum_i \left( \text{ALK}^{\text{NIT}} \cdot \frac{\gamma_{\text{NH}_4}}{1+K_{\text{NH}_4}} \text{NC}_i + \text{ALK}^{\text{OX}} \right) \cdot k_i \cdot C_i(z) \end{aligned} \quad (23)$$

435 2. Layer ( $z_{\text{ox}} < z \leq z_{\text{NO}_3}$ )

$$\frac{\partial \text{ALK}^{II}}{\partial t} = 0 = D_{\text{ALK}} \frac{\partial^2 \text{ALK}^{II}}{\partial z^2} - w \frac{\partial \text{ALK}^{II}}{\partial z} + \frac{1-\phi}{\phi} \cdot \sum_i \text{ALK}^{\text{DEN}} \cdot k_i \cdot C_i(z) \quad (24)$$

3. Layer ( $z_{\text{NO}_3} < z \leq z_{\text{SO}_4}$ )

$$\frac{\partial \text{ALK}^{III}}{\partial t} = 0 = D_{\text{ALK}} \frac{\partial^2 \text{ALK}^{III}}{\partial z^2} - w \frac{\partial \text{ALK}^{III}}{\partial z} + \frac{1-\phi}{\phi} \cdot \sum_i \text{ALK}^{\text{SUL}} \cdot k_i \cdot C_i(z) \quad (25)$$

440

4. Layer ( $z_{\text{SO}_4} < z \leq z_{\infty}$ )

$$\frac{\partial \text{ALK}^{IV}}{\partial t} = 0 = D_{\text{ALK}} \frac{\partial^2 \text{ALK}^{IV}}{\partial z^2} - w \frac{\partial \text{ALK}^{IV}}{\partial z} + \frac{1-\phi}{\phi} \cdot \sum_i \text{ALK}^{\text{MET}} \cdot k_i \cdot C_i(z) \quad (26)$$

To solve equations 23 - 26 the model assumes a known concentration at the sediment-water interface  
 445 and continuity across the bioturbation depth and the penetration depths of  $\text{O}_2$ ,  $\text{NO}_3$  and  $\text{SO}_4$  (see  
 Table 8). The decrease of alkalinity due to oxidation of reduced species produced in the suboxic and  
 anoxic layers (with stoichiometry  $\text{ALK}^{\text{NIT}}$  and  $\text{ALK}^{\text{H}_2\text{S}}$ ) is implicitly taken into account through  
 the flux boundary condition at  $z_{\text{ox}}$  (Table 8 Eq. 5). Furthermore, the oxidation of methane by sulphate  
 reduction increases alkalinity with stoichiometry  $\text{ALK}^{\text{AOM}}$  which is accounted for through the flux  
 450 boundary condition at  $z_{\text{SO}_4}$  (Table 8 eq. 9). At the lower boundary  $z_{\infty}$  a zero flux condition is  
 applied.

## 2.4 Model Parameters

This section describes the parameters used in OMEN-SED to describe sediment transport and bio-  
 geochemical reactions related to the burial and mineralization of organic matter under a wide range  
 455 of environmental conditions. Table 9 states the parameters for sediment characteristics and table 10  
 summarizes the stoichiometric factors and secondary reaction parameters used in the model.

### 2.4.1 Transport Parameters

Advection is the bulk flow of sediments and can be directly related to the accumulation of new  
 material on the seafloor (i.e. sedimentation, Burdige, 2006). This results in a downward flux of older  
 460 sediment material and porewater in relation to the sediment-water interface. When coupled to an  
 ocean model, its sedimentation flux can be readily used in OMEN-SED 1.0. The stand-alone version

**Table 8.** Boundary conditions for alkalinity. For the boundaries we define:  $z_-^- := \lim_{h \rightarrow 0} (z_- - h)$  and  $z_-^+ := \lim_{h \rightarrow 0} (z_- + h)$ .

Boundary	Condition	
$z = 0$	known concentration	1) $ALK(0) = ALK_0$
$z = z_{\text{bio}}$	continuity	2) $ALK(z_{\text{bio}}^-) = ALK(z_{\text{bio}}^+)$
	flux	3) $-(D_{\text{ALK},0} + D_{\text{bio}}) \cdot \frac{\partial ALK}{\partial z} \Big _{z_{\text{bio}}^-} = -D_{\text{ALK},0} \cdot \frac{\partial ALK}{\partial z} \Big _{z_{\text{bio}}^+}$
$z = z_{\text{ox}}$	continuity	4) $ALK(z_{\text{ox}}^-) = ALK(z_{\text{ox}}^+)$
	flux	5) $-D_{\text{ALK}} \cdot \frac{\partial ALK}{\partial z} \Big _{z_{\text{ox}}^-} + F_{\text{ALK}}(z_{\text{ox}}) = -D_{\text{ALK}} \cdot \frac{\partial ALK}{\partial z} \Big _{z_{\text{ox}}^+}$
	where:	$F_{\text{ALK}}(z_{\text{ox}}) = \frac{1-\phi}{\phi} \cdot \left( ALK^{\text{H}_2\text{S}} \cdot \gamma_{\text{H}_2\text{S}} \int_{z_{\text{NO}_3}}^{z_{\text{SO}_4}} \sum_i \text{SO}_4\text{C} \cdot k_i \cdot C_i dz \right) + \frac{1-\phi}{\phi} \cdot \left( ALK^{\text{NIT}} \frac{\gamma_{\text{NH}_4}}{1+k_{\text{NH}_4}} \int_{z_{\text{NO}_3}}^{\infty} \sum_i \text{NC}_i \cdot k_i \cdot C_i dz \right)$
$z = z_{\text{NO}_3}$	continuity	6) $ALK(z_{\text{NO}_3}^-) = ALK(z_{\text{NO}_3}^+)$
	flux	7) $-D_{\text{ALK}} \cdot \frac{\partial ALK}{\partial z} \Big _{z_{\text{NO}_3}^-} = -D_{\text{ALK}} \cdot \frac{\partial ALK}{\partial z} \Big _{z_{\text{NO}_3}^+}$
$z = z_{\text{SO}_4}$	continuity	8) $ALK(z_{\text{SO}_4}^-) = ALK(z_{\text{SO}_4}^+)$
	flux (with AOM)	9) $-D_{\text{ALK}} \cdot \frac{\partial ALK}{\partial z} \Big _{z_{\text{SO}_4}^-} + F_{\text{ALK}}(z_{\text{SO}_4}) = -D_{\text{ALK}} \cdot \frac{\partial ALK}{\partial z} \Big _{z_{\text{SO}_4}^+}$
	where:	$F_{\text{ALK}}(z_{\text{SO}_4}) = \frac{1-\phi}{\phi} \cdot \left( ALK^{\text{AOM}} \gamma_{\text{CH}_4} \cdot \int_{z_{\text{SO}_4}}^{\infty} \sum_i k_i \cdot C_i dz \right)$
$z = z_{\infty}$	zero ALK flux	10) $\frac{\partial ALK}{\partial z} \Big _{z_{\infty}} = 0$

of OMEN-SED 1.0 uses the empirical global relationship between sediment accumulation rate ( $\text{cm yr}^{-1}$ ) and seafloor depth (m) of Middelburg et al. (1997):

$$w = 3.3 \cdot 10^{-0.87478367 - 0.00043512 \cdot \text{depth}}, \quad (27)$$

465 As discussed before (Sec. 2.2), the diffusion coefficient of species  $i$  is calculated as  $D_i = D_{i,0} + D_{\text{bio}} = D_{\text{mol},i} \cdot f_{ir} + D_{\text{bio}}$  for dissolved species and  $D_i = D_{\text{bio}}$  for solid species. The bioturbation coefficient  $D_{\text{bio}}$  ( $\text{cm}^2 \text{ yr}^{-1}$ ) is constant in the bioturbated zone and also follows the empirical relationship by Middelburg et al. (1997):

$$D_{\text{bio}} = 5.2 \cdot 10^{0.76241122 - 0.00039724 \cdot \text{depth}} \quad (28)$$

470 Studies showed that bioturbational effects on a global scale are largely restricted to the upper 10 cm of the sediments and are only marginally related to seafloor depth (e.g. Boudreau, 1998; Teal et al., 2010). Therefore, OMEN-SED imposes a globally invariant bioturbation depth  $z_{\text{bio}}$  of 10 cm. In case the bottom water oxygen concentration is below 5 nanomole  $\text{cm}^{-3}$  infaunal activity ceases and  $z_{\text{bio}} = 0.01 \text{ cm}$ .

475 Bioirrigation can enhance the molecular diffusion coefficient  $D_{i,0} = D_{\text{mol},i} \cdot f_{ir}$  (Soetaert et al., 1996a). However, here we do not consider this effect and set  $f_{ir}$  to a constant value of 1. The specific molecular diffusion coefficients  $D_{\text{mol},i}$  are corrected for sediment porosity  $\phi$ , tortuosity  $F$  and are linearly interpolated for an ambient temperature  $T$  using zero-degree coefficients  $D_i^0$  and

temperature-dependent diffusion coefficients  $D_i^T$  (compare Gypens et al., 2008):

$$D_{\text{mol},i} = (D_i^0 + D_i^T \cdot T) \cdot \frac{1}{\phi \cdot F}$$

Tortuosity can be expressed in terms of porosity as  $F = \frac{1}{\phi^m}$  (Ullman and Aller, 1982) with the exponent  $m$  varying according to the type of sediment (here we use  $m=3$ ). Values for  $D_i^T$  and  $D_i^0$  are summarized in Table 9 and are adapted from Li and Gregory (1974) and Gypens et al. (2008).

#### 2.4.2 Reaction Parameters and Stoichiometries

The applied multi-G approach for organic matter degradation considers specific degradation rate constants  $k_i$  ( $\text{yr}^{-1}$ ) for each compound class which are assumed invariant along the sediment column and therefore independent of the nature of the terminal electron acceptor. The rate constants can be altered manually to fit observed sediment profiles (compare Section 3.1) or related to a master variable (e.g. sedimentation rate or POC-flux) provided by a coupled Earth System Model (compare Section 2.5.2 and 3.3). The rate constants for P related processes (i.e. sorption of  $\text{PO}_4$  to Fe oxides, release of  $\text{PO}_4$  from Fe-bound P due to Fe-oxide reduction and authigenic CFA precipitation) are  $k_s$ ,  $k_m$ ,  $k_a$  respectively. The pore water equilibrium concentrations for P sorption and CFA precipitation ( $\text{PO}_4^s$ ,  $\text{PO}_4^a$ ) and the asymptotic concentration for Fe-bound P ( $M^\infty$ ) are taken from the Slomp et al. (1996). The stoichiometry of organic matter is represented by the factors  $\text{NC}_i$  and  $\text{PC}_i$  denoting the molecular nitrogen to carbon and phosphorus to carbon ratio. In the sulfidic and methanic zone the reduction of 1 mol organic matter additionally produces  $\text{SO}_4\text{C} = \frac{138}{212}$  mol of hydrogen sulfide and  $\text{MC} = 0.5$  mol of methane. In the total sediment column organic matter mineralization consumes the specific TEA with a fixed ratio ( $\text{O}_2\text{C}$ ,  $\text{NO}_3\text{C}$  and  $\text{SO}_4\text{C}$  respectively). See Table 10 for a complete summary of the parameters and their values.

### 2.5 Module Structure

An analytical steady-state solution is found for the reaction-transport equation of each chemical species for every layer. At each boundary (i.e.  $z_{\text{ox}}$ ,  $z_{\text{bio}}$ ,  $z_{\text{NO}_3}$  and  $z_{\text{SO}_4}$ ) the model has to match continuity and flux for the ODE solutions of the layer above and below the specific boundary. In particular the bioturbation boundary is problematic as it can theoretically occur in any geochemical layer (compare Fig. 3). In order to simplify this recurring boundary matching problem it is implemented in an independent algorithm which is described in Section 2.5.1. Instructions and requirements for coupling OMEN-SED to a global Earth Sytem Model are given in Section 2.5.2.

#### 2.5.1 Generic Boundary Condition Matching (GBCM)

A general steady-state advection-diffusion-reaction (ADR) diagenetic equation looks like:

$$\frac{\partial C}{\partial t} = 0 = D \frac{\partial^2 C}{\partial z^2} - w \frac{\partial C}{\partial z} - \sum_i \alpha_i \exp(-\beta_i z) - k \cdot C + Q. \quad (29)$$

**Table 9.** Sediment characteristics and transport parameters. **TODO: PO4 adsorption coefficients okay?**

Parameter	Unit	Value	Description/Source
$\rho_{\text{sed}}$	$\text{g cm}^{-3}$	2.6	Sediment density
$w$	$\text{cm yr}^{-1}$	Fct. of seafloor depth or from ESM	Advection/Sediment accumulation rate (Middelburg et al., 1997)
$z_{\text{bio}}$	cm	10 or 0.01	Bioturbation depth (Boudreau, 1998; Teal et al., 2010)
$D_{\text{bio}}$	$\text{cm}^2 \text{yr}^{-1}$	Fct. of seafloor depth	Bioturbation coefficient (Middelburg et al., 1997)
$\phi$	-	0.85	Porosity
$F$	-	$\frac{1}{\phi^m}$	Tortuosity, here $m=3$
$f_{ir}$	-	1	Irrigation factor
<b>Adsorption coefficients</b>			
$K_{\text{NH}_4}$	-	1.3	$\text{NH}_4$ adsorption coefficient, (see Wang and Van Cappellen, 1996)
$K_{\text{PO}_4}^{\text{ox}}$	-	200.0	$\text{PO}_4$ adsorption coefficient (oxic), (see Slomp et al., 1998)
$K_{\text{PO}_4}^{\text{anox}}$	-	1.3	$\text{PO}_4$ adsorption coefficient (anoxic), (see Slomp et al., 1998)
<b>Diffusion coefficients</b> (Li and Gregory, 1974; Schulz, 2006; Gypens et al., 2008)			
$D_{\text{O}_2}^0$	$\text{cm}^2 \text{yr}^{-1}$	348.62	Molecular diffusion coefficient of oxygen at $0^\circ\text{C}$
$D_{\text{O}_2}^T$	$\text{cm}^2 \text{yr}^{-1} \text{ } ^\circ\text{C}^{-1}$	14.09	Diffusion coefficient for linear temp. dependence of oxygen
$D_{\text{NO}_3}^0$	$\text{cm}^2 \text{yr}^{-1}$	308.42	Molecular diffusion coefficient of nitrate at $0^\circ\text{C}$
$D_{\text{NO}_3}^T$	$\text{cm}^2 \text{yr}^{-1} \text{ } ^\circ\text{C}^{-1}$	12.26	Diffusion coefficient for linear temp. dependence of nitrate
$D_{\text{NH}_4}^0$	$\text{cm}^2 \text{yr}^{-1}$	309.05	Molecular diffusion coefficient of ammonium at $0^\circ\text{C}$
$D_{\text{NH}_4}^T$	$\text{cm}^2 \text{yr}^{-1} \text{ } ^\circ\text{C}^{-1}$	12.26	Diffusion coefficient for linear temp. dependence of ammonium
$D_{\text{SO}_4}^0$	$\text{cm}^2 \text{yr}^{-1}$	157.68	Molecular diffusion coefficient of sulfate at $0^\circ\text{C}$
$D_{\text{SO}_4}^T$	$\text{cm}^2 \text{yr}^{-1} \text{ } ^\circ\text{C}^{-1}$	7.88	Diffusion coefficient for linear temp. dependence of sulfate
$D_{\text{H}_2\text{S}}^0$	$\text{cm}^2 \text{yr}^{-1}$	307.48	Molecular diffusion coefficient of sulfide at $0^\circ\text{C}$
$D_{\text{H}_2\text{S}}^T$	$\text{cm}^2 \text{yr}^{-1} \text{ } ^\circ\text{C}^{-1}$	9.64	Diffusion coefficient for linear temp. dependence of sulfide
$D_{\text{PO}_4}^0$	$\text{cm}^2 \text{yr}^{-1}$	112.91	Molecular diffusion coefficient of phosphate at $0^\circ\text{C}$
$D_{\text{PO}_4}^T$	$\text{cm}^2 \text{yr}^{-1} \text{ } ^\circ\text{C}^{-1}$	5.59	Diffusion coefficient for linear temp. dependence of phosphate
$D_{\text{DIC}}^0$	$\text{cm}^2 \text{yr}^{-1}$	181.96	Molecular diffusion coefficient of DIC at $0^\circ\text{C}$
$D_{\text{DIC}}^T$	$\text{cm}^2 \text{yr}^{-1} \text{ } ^\circ\text{C}^{-1}$	8.66	Diffusion coefficient for linear temp. dependence of DIC
$D_{\text{ALK}}^0$	$\text{cm}^2 \text{yr}^{-1}$	181.96	Molecular diffusion coefficient of ALK at $0^\circ\text{C}$
$D_{\text{ALK}}^T$	$\text{cm}^2 \text{yr}^{-1} \text{ } ^\circ\text{C}^{-1}$	8.66	Diffusion coefficient for linear temp. dependence of ALK
Note: DIC and ALK coefficients are the mean values of $\text{HCO}_3^-$ , $\text{CO}_3^{2-}$ and $\text{CO}_2$ from Schulz (2006).			

**Table 10.** Values for biogeochemical parameters used in OMEN-SED. The variables  $x$ ,  $y$  and  $z$  denote the atomic ratio of carbon, nitrogen and phosphorous of the degrading organic matter (here set to  $C : N : P = 106 : 16 : 1$ ). **P related coefficients okay?**

Parameter/Variable	Unit	Value	Description
<b>Stoichiometric factors and molecular ratios</b>			
$NC_i$	mol/mol	$\frac{y}{x} = \frac{16}{106}$	nitrogen to carbon ratio
$PC_i$	mol/mol	$\frac{z}{x} = \frac{1}{106}$	phosphorus to carbon ratio
$MC$	mol/mol	0.5	methane to carbon ratio
			produced during methanogenesis
$DICC^I$	mol/mol	1.0	DIC to carbon ratio until $z_{SO_4}$
$DICC^{II}$	mol/mol	0.5	DIC to carbon ratio below $z_{SO_4}$
$O_2C$	mol/mol	$\frac{x+2y}{x} = \frac{138}{106}$	oxygen to carbon ratio
$NO_3C$	mol/mol	$\frac{4x+3y}{5x} = \frac{94.4}{106}$	nitrate to carbon ratio
$SO_4C$	mol/mol	$\frac{1}{2} O_2C = \frac{138}{212}$	sulfate to carbon ratio
$ALK^{OX}$	mol/mol	$\frac{y-2z}{x} = \frac{14}{106}$	ALK from aerobic degradation
$ALK^{NIT}$	mol/mol	-2	ALK from nitrification
$ALK^{DEN}$	mol/mol	$\frac{4x+3y-10z}{5x} = \frac{92.4}{106}$	ALK from denitrification
$ALK^{SUL}$	mol/mol	$\frac{x+y-2z}{x} = \frac{120}{106}$	ALK from sulfate reduction
$ALK^{MET}$	mol/mol	$\frac{y-2z}{x} = \frac{14}{106}$	ALK from methanogenesis
$ALK^{H_2S}$	mol/mol	-2	ALK from $H_2S$ oxidation
$ALK^{AOM}$	mol/mol	2	ALK from AOM
<b>Secondary reaction parameters</b>			
$\gamma_{NH_4}$	-	0.9	fraction of $NH_4$ that is oxidised in oxic layer
$\gamma_{H_2S}$	-	0.95	fraction of $H_2S$ that is oxidised in oxic layer
$\gamma_{CH_4}$	-	0.99	fraction of $CH_4$ that is oxidised at $z_{SO_4}$
<b>P related parameters</b>			
$k_s$	$yr^{-1}$	1.0	Rate constant for $PO_4$ sorption
$k_m$	$yr^{-1}$	0.02	Rate constant for Fe-bound P release
$k_a$	$yr^{-1}$	10.0	Rate constant for authigenic CFA precipitation
$PO_4^s$	$mol\ cm^{-3}$	$1 \cdot 10^{-9}$	equilibrium conc. for P sorption (Slomp et al., 1996)
$PO_4^a$	$mol\ cm^{-3}$	$3.7 \cdot 10^{-9}$	equilibrium conc. for authigenic P precipitation (Slomp et al., 1996)
$M^\infty$	$mol\ cm^{-3}$	$1.99 \cdot 10^{-10}$	asymptotic concentration for Fe-bound P (Slomp et al., 1996)

**DH:**  $ALK^{OX}$  correct?:  
 $y = NH_4$  prod.;  $-2z = P$   
release

where  $z$  is the sediment depth,  $t$  the time,  $D$  is the diffusion coefficient and  $w$  is the advection rate. The ODE solution is of the general form:

$$C(z) = A \exp(az) + B \exp(bz) + \sum_i \frac{\alpha_i}{D\beta_i^2 - w\beta_i - k} \cdot \exp(-\beta_i z) + \frac{Q}{k} \quad (30)$$

and can therefore be expressed as:

$$C(z) = A \cdot E(z) + B \cdot F(z) + G(z) \quad (31)$$

where  $E(z)$ ,  $F(z)$  are the homogeneous solutions of the ODE,  $G(z)$  the particular integral, and  $A$ ,  $B$  are the integration constants (compare Fig. 3 for the whole sediment column).

Each boundary matching problem involves matching continuity and flux for the two solutions  $C_U(z)$  (= 'upper') and  $C_L(z)$  (= 'lower') across a boundary at  $z = z_b$ . Therefore, we get two ODE solutions of the genral form:

$$C_U(z) = A_U \cdot E_U(z) + B_U \cdot F_U(z) + G_U(z) \quad (32)$$

$$C_L(z) = A_L \cdot E_L(z) + B_L \cdot F_L(z) + G_L(z). \quad (33)$$

The two boundary conditions are: for continuity (where for generality we allow a discontinuity  $V_b$ )

$$C_U(z_b) = C_L(z_b) + V_b \quad (34)$$

and for flux

$$D_U C'_U(z_b) + w C_U(z_b) = D_L C'_L(z_b) + w C_L(z_b) + F_b \quad (35)$$

where  $w$  is advection,  $D$  are the diffusion coefficients and  $F_b$  is any flux discontinuity.

In terms of the ODE solutions (32), (33), the boundary conditions represent two equations connecting the four integration constants:

$$\begin{pmatrix} E_U & F_U \\ D_U E'_U & D_U F'_U \end{pmatrix} \begin{pmatrix} A_U \\ B_U \end{pmatrix} = \begin{pmatrix} E_L & F_L \\ D_L E'_L & D_L F'_L \end{pmatrix} \begin{pmatrix} A_L \\ B_L \end{pmatrix} + \begin{pmatrix} G_L - G_U + V_b \\ D_L G'_L - D_U G'_U + F_b - w V_b \end{pmatrix} \quad (36)$$

where the ODE solutions  $E$ ,  $F$ ,  $G$  are all evaluated at  $z_b$ .

Equation (36) can be solved to give  $A_U$  and  $B_U$  as a function of the integration constants from the layer below ( $A_L$  and  $B_L$ ), thereby constructing a piecewise solution for both layers, with just two integration constants.



In the code the function **benthic\_utils.matchsoln** provides this solution in the form:

$$\begin{pmatrix} A_U \\ B_U \end{pmatrix} = \begin{pmatrix} c_1 & c_2 \\ c_3 & c_4 \end{pmatrix} \begin{pmatrix} A_L \\ B_L \end{pmatrix} + \begin{pmatrix} d_1 \\ d_2 \end{pmatrix}. \quad (37)$$

Using (37) we can now rewrite  $C_U(z)$  in (32) as a function of  $A_L$  and  $B_L$ :

$$545 \quad C_U(z) = (c_1 A_L + c_2 B_L + d_1) \cdot E_U(z) + (c_3 A_L + c_4 B_L + d_2) \cdot F_U(z) + G_U(z)$$

and hence define the “transformed” basis functions  $E_U^*(z)$ ,  $F_U^*(z)$ ,  $G_U^*(z)$  such that:

$$C_U(z) = A_L \cdot E_U^*(z) + B_L \cdot F_U^*(z) + G_U^*(z) \quad (38)$$

where

$$E_U^*(z) = c_1 E_U(z) + c_3 F_U(z)$$

$$550 \quad F_U^*(z) = c_2 E_U(z) + c_4 F_U(z) \quad (39)$$

$$G_U^*(z) = G_U(z) + d_1 E_U(z) + d_2 F_U(z)$$

(in the code this is done by **benthic\_utils.xformsoln**).

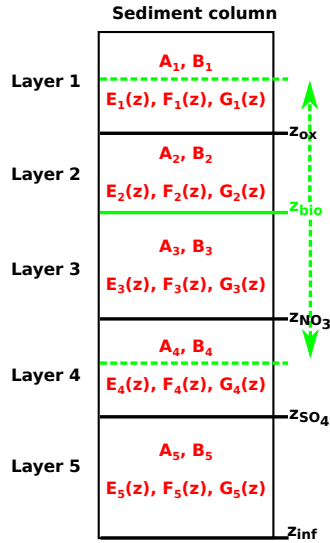


**Figure 3.** Schematic of the generic boundary condition matching (GBCM) problem. Showing the resulting integration constants ( $A_i$ ,  $B_i$ ) and ODE solutions ( $E_i$ ,  $F_i$ ,  $G_i$ ) for the different sediment layers and the variable bioturbation boundary.

### Solving the sediment layer stack

555 Equations (37), (38) and (39) can now be applied for each layer boundary, working up from the bottom of the sediments. The net result is a piecewise solution of the whole sediment column with

just two integration constants (coming from the lowest layer), which can then be solved for by applying one boundary condition for the sediment-water interface and one for the bottom of the sediments (e.g. a concentration condition at the SWI and a zero flux condition at  $z_{\infty}$ ).

## 560 Abstracting out the bioturbation boundary

The bioturbation boundary affects the diffusion coefficient of the modelled solutes and the conservation equation of organic matter. The boundary is particularly inconvenient as it can, in principle, occur in the middle of any “geochemical” layer and therefore generates multiple cases (compare Fig. 3). To simplify this for solutes, the GBCM algorithm above is used to construct a piecewise solution  
565 and to abstract out the bioturbation boundary. An initial test for each “geochemical” layer is made to identify its “bioturbation-status” (fully bioturbated, fully non-bioturbated or crossing the bioturbation boundary) and (if needed) a piecewise solution is constructed by matching boundary conditions across the bioturbation boundary. The “outside” code therefore never needs to know whether it is dealing with a piecewise solution (i.e. matched across a bioturbation boundary) or a “simple” solution  
570 (i.e. the layer is fully bioturbated or fully non-bioturbated).

In the code, this is performed by **zTOC.prepfg\_I12** which hands back a structure **ls** containing the “bioturbation-status” for each layer and (if needed) the description of the piecewise solution (coefficients  $c_1, c_2, c_3, c_4, d_1, d_2$  as above). For example in the case of sulfate, **zTOC.prepfg\_I12** is called three times before the actual profile is calculated (once per layer: oxic, suboxic, sulfidic) and hands  
575 back three structures **ls** with information about the layer’s “bioturbation-status” and all associated conditional logic. When calculating the solutions for the different layers, the pre-calculated structure **ls** is passed to the function **zTOC.calcfg\_I12** which sorts out the correct solution type to use.

### 2.5.2 Coupling to an Earth System Model

The coupling of OMEN-SED to the carbon-centric version of the “GENIE” Earth system model  
580 (cGENIE Ridgwell et al., 2007) is described (Fig. 4). Results from pre-industrial experiments are presented in Section 3.3. cGENIE is a model of Intermediate Complexity based on the efficient climate model “C-GOLDSTEIN” of Edwards and Marsh (2005), featuring a frictional-geostrophic 3D-ocean circulation model coupled to a fast Energy-Moisture Balance 2D-atmosphere together with a dynamic-thermodynamic sea-ice component. The version of cGENIE used here includes the marine  
585 geochemical cycling of carbon, oxygen, phosphorus and sulfur (Ridgwell et al., 2007), preservation of carbonates in deep-sea sediments (Ridgwell and Hargreaves, 2007) and terrestrial weathering (Colbourn et al., 2013). The ocean model is implemented on a  $36 \times 36$  equal-area horizontal grid with 16 vertical levels using the pre-industrial continental configuration and bathymetry as in Archer et al. (2009). In contrast to Archer et al. (2009) the same grid resolution ( $36 \times 36$ ) is used for  
590 the sediment geochemistry model SEDGEM. Instead of completely degrading POC at the seafloor, OMEN-SED is called by SEDGEM for each grid point. Depending on the overlying biogeochemical

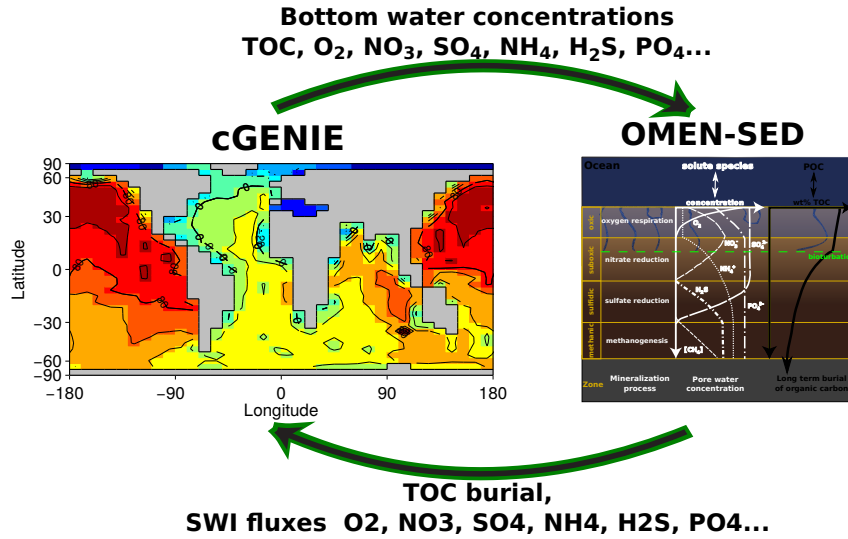


**Figure 4.** Schematic of the relationship between OMEN-SED and cGENIE. Arrows and accompanied text represent the information transferred between models.

ocean model processes can be included or excluded in OMEN-SED and stoichiometric factors need to be adjusted to ensure preservation of mass. As nitrogen is not modelled explicitly in the employed cGENIE configuration the related stoichiometries in OMEN-SED are set to zero (i.e.  $NC_i$ ,  $ALK^{NIT}$  and  $ALK^{DEN}$ ). cGENIE, however, implicitly includes the effects of  $NH_4$  release and its nitrification on Alkalinity and neglects the impact of P release; therefore, related stoichiometries are changed to  $ALK^{OX} = -16/106$  and  $ALK^{SUL} = 122/106$ .

Several biogeochemical tracers and parameters are transferred from SEDGEM to OMEN-SED and have to be converted into the required units. Bottom water concentrations of solutes are converted from  $\text{mol kg}^{-1}$  to  $\text{mol cm}^{-3}$  and the depositional flux of POC ( $POC_{\text{flux}}$ ) is converted from  $\text{cm}^3 \text{cm}^{-2} \text{yr}^{-1}$  to  $\text{mol cm}^{-2} \text{yr}^{-1}$  assuming an average density of POC of  $1.0 \text{ cm}^3 \text{g}^{-1}$ . Other parameters used from cGENIE are seafloor depth, local temperature and the partitioning of bulk POC into the slower and faster degrading pool (as cGENIE represents a labile and a refractory POC fraction, see Ridgwell et al. (2007)). The advection/sediment accumulation rate is generally taken from cGENIE, however, a minimum values of  $w = 0.5 \text{ cm kyr}^{-1}$  is imposed as OMEN-SED tends to be unstable for lower values. The bulk  $POC_{\text{flux}}$  is separated into the labile and refractory component and the routine to calculate the sedimentary POC profiles is called. Here, the two POC depositional fluxes are first converted into SWI concentrations (in  $\text{mol cm}^{-3}$ ) by solving Eq. (3) for  $z=0$ . OMEN-SED computes the resulting SWI-fluxes of solutes (in  $\text{mol cm}^{-2} \text{yr}^{-1}$ ) and the fraction of POC preserved in the sediment at a depth of 100 cm ( $POC_{\text{pres}}$ ) and returns the results to cGENIE. In case no POC is deposited on the seafloor (i.e.  $POC_{\text{flux}} = 0$ ), OMEN-SED is not called and the SWI-fluxes of solutes and  $POC_{\text{pres}}$  are set to zero. In order to reduce memory requirements the sed-

iment profiles (e.g. as shown in Fig. 5) are not calculated in the FORTRAN version of OMEN-SED, however, the boundary conditions are saved at the end of the experiment and sediment profiles for specific grid-cells, ocean basins and/or ocean transects can be plotted using the stand-alone matlab version of OMEN-SED.

### 3 Model Applications

**TODO: Check Intro sentences** To validate our approach, model results were compared with observed pore water profiles (Section 3.1), an extensive sensitivity analysis for the most important model parameters was performed and resulting sediment-water interface fluxes were compared with a global database (Section 3.2). Furthermore, OMEN-SED was coupled to the cGENIE Earth System model and different published parameterisations for the OM degradation rate constants are tested on a global scale (Section 3.3).

#### 3.1 Sediment profiles

Modelled profiles were compared with measured pore water data from different ocean depths (Figure 5) including the continental shelf (108 m), upper slope (585 m), lower slope (2213 m) and the deep sea (4298 m). The site at 585 m depth located in the Santa Barbara Basin is characterised by anoxic bottom waters and high POC concentrations (POC  $\sim$ 5.5 wt%, Reimers et al., 1996), whereas the other sites at the Iberian margin (108 and 2213 m) and the Nazaré Canyon (4298 m, Epping et al., 2002) are oxic. Sediment-water interface characteristics and concentrations of POC and dissolved species in OMEN-SED were set to the observed values where available (Table 11). The POC and pore water profiles were fitted by optimizing the POC partitioning into the fast and slow degrading pool and their respective first order degradation rate constants (priority given to reproduce the POC and O<sub>2</sub> profiles). For phosphorus the equilibrium concentration for authigenic P formation (PO<sub>4</sub><sup>a</sup>) was adjusted to fit the PO<sub>4</sub> concentration at  $z_{\infty}$ . For the two open Iberian margin stations (108 and 2213 m) OMEN-SED fits all observations well. OMEN-SED does especially well at depth 2213m by reproducing the deep O<sub>2</sub> penetration and the subsurface maximum in NO<sub>3</sub> concentration due to the nitrification of NH<sub>4</sub>. For the Santa Barbara basin (585 m) a misfit is observed for H<sub>2</sub>S and PO<sub>4</sub> in the upper 20 cm of the sediment. This can be explained by the presence of Mn<sup>2+</sup>, Fe<sup>2+</sup> and dissolved Fe at this site which are either reduced to degrade POC and/or react with H<sub>2</sub>S to form iron sulfides, therefore inhibiting the rise in concentration of H<sub>2</sub>S (Reimers et al., 1996). Phosphorus is adsorbed to Fe oxides and incorporated into carbonate fluorapatite (CFA) which is highly parameterised in OMEN-SED and not modelled explicitly. For the Nazaré Canyon station (4298 m) satisfactory fits could be realised apart from NH<sub>4</sub>. However, also the original study (Epping et al., 2002) had the same problem using a more complex diagenetic model and suggested non-local solute exchange being responsible for the higher NH<sub>4</sub> concentrations at this site.

**DH: P explanation correct/okay?**  
**Also, say something about [ALK] at 585m?**

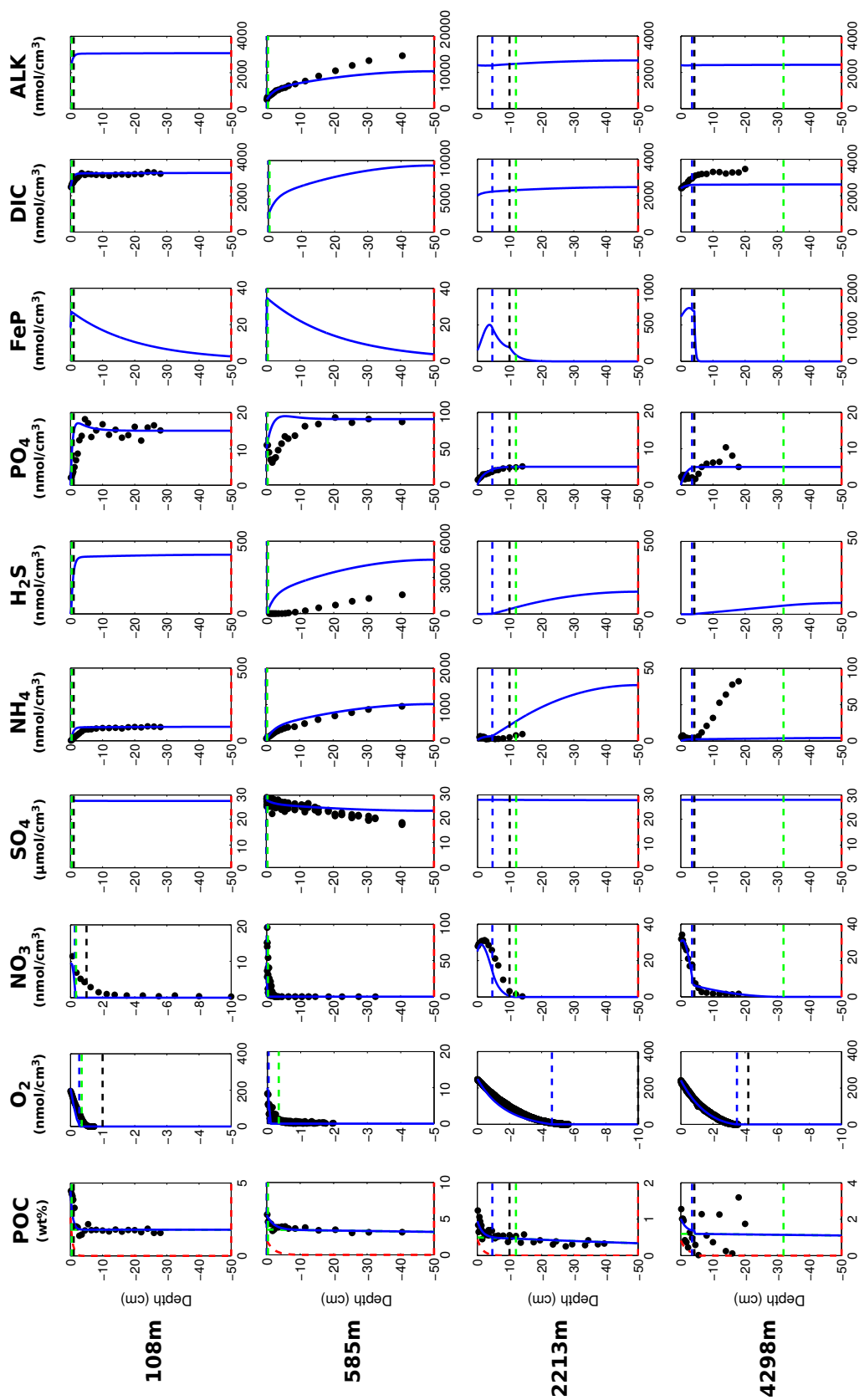


**Figure 5.** Modelled (curves) and measured (filled dots) dissolved and solid phase pore water profiles for four different sediment cores. Note that different scales are used for different stations. The blue POC curve represents the sum of the refractory (green) and labile (red) POC fraction.

**Table 11.** Model boundary conditions for the sampling stations in Figure 5. (For all sites DIC bottom water concentration of 2,400 nanomole  $\text{cm}^{-3}$  is assumed.)

Sediment characteristics:								
Depth	Temp.	$z_{\text{bio}}$	$D_{\text{bio}}$	POC <sub>1</sub>	POC <sub>2</sub>	k <sub>1</sub>	k <sub>2</sub>	
(m)	(°C)	(cm)	(cm <sup>2</sup> yr <sup>-1</sup> )	(wt%)	(wt%)	(yr <sup>-1</sup> )	(yr <sup>-1</sup> )	
108	12.5	1.0	0.02	2.64	1.8	0.65	1.0e <sup>-5</sup>	
585	5.85	0.01	0.02	2.0	3.5	0.2	8.0e <sup>-4</sup>	
2213	3.2	10.0	0.17	0.45	0.5	0.1	4.0e <sup>-4</sup>	
4298	2.5	4.2	0.18	0.83	1.2	0.052	1e <sup>-5</sup>	
Bottom water concentrations of solutes (all in nanomole cm <sup>-3</sup> ):								
Depth	O <sub>2</sub>	NO <sub>3</sub>	SO <sub>4</sub>	NH <sub>4</sub>	H <sub>2</sub> S	PO <sub>4</sub>	PO <sub>4</sub> <sup>a</sup>	Alkalinity
108	210	9.6	28,000	0.4	0.0	0.0	15.0	2,400
585	10	25.0	28,000	0.0	0.0	50.0	90.0	2,480
2213	250	25.0	28,000	0.6	0.0	0.0	5.0	2,400
4298	243	30.1	28,000	0.22	0.0	0.0	5.0	2,400

### 3.2 Sensitivity Analysis

Model parameters implicitly account for processes not explicitly described, they are notoriously difficult to constrain and a source of uncertainty for numerical and analytical models. One strategy to explore and quantify this model uncertainty that can always be applied is sensitivity analysis (SA). SA is a term used for mathematical techniques to investigate how the variations in the outputs ( $y_1, \dots, y_N$ ) of a model can be attributed to variations in the different input parameters ( $x_1, \dots, x_M$ ) (Pianosi et al., 2016). Different types of sensitivity indices, which quantify this relative influence with a scalar  $S_i$ , can be calculated, ranging from simple one-at-a-time methods to statistical evaluations of the output distribution (e.g. variance-based or density-based approaches Pianosi et al., 2016). Especially the latter indices are easy to interpret and can be compared across different parameters and/or different model outputs as they generally take values between zero and one ( $S_i \in [0, 1]$ ). An index of zero indicates a non-influential parameter and a higher value a more influential parameter. Here, we use SA mainly to identify which parameters have the largest impact on the different model outputs and therefore require careful calibration. As the probability density functions of our model outputs (i.e. the resulting SWI-fluxes) are generally highly-skewed towards extreme organic matter degradation rates (not shown) variance-based sensitivity indices are not very reliable uncertainty indicators (Pianosi et al., 2016). Rather than just considering the variance we employ the novel density-based PAWN method by (Pianosi and Wagener, 2015) which considers the entire conditional and unconditional Cumulative Distribution Function (CDF) of the model output. The sensitivity in-

dex of parameter  $i$  is calculated as the difference between the two CDFs, i.e.

$$S_i = \max_{x_i} \max_y |F_y(y) - F_{y|x_i}(y)| \quad (40)$$

where  $F_y(y)$  is the unconditional CDF of the output  $y$  and  $F_{y|x_i}(y)$  represents the conditional CDF when the  $i$ -th parameter is fixed to  $x_i$ . For a more detailed description of the method we refer the

interested reader to Pianosi and Wagener (2015).

Due to the model complexity it is impossible to compute the sensitivity indices analytically therefore they are approximated from a Latin-Hypercube sampling of parameter inputs and calculated outputs. The PAWN method, as implemented within the Sensitivity Analysis for Everyone (SAFE) matlab toolbox (Pianosi et al., 2015), is used to investigate 11 model parameters for ranges as specified in Table 12. Sensitivity indices for all resulting SWI-fluxes for two idealised sediment conditions (i.e. anoxic at 400 m and oxic at 4000 m, see Table 13) are calculated. We use 200 samples to estimate the unconditional CDF, 100 samples to estimate the conditional CDFs and 10 conditioning points, thus 11,200 evaluations are performed for each sediment condition. The resulting indices (compare Fig. 9 in the Appendix) are then translated into a color code and summarised in a pattern plot to simplify comparison (Fig. 6). The most significant parameters for all model outputs are the degradation rate for the labile OM part ( $k_1$ ) and its share in the total OM pool ( $f_1$ ). For the anoxic setup, where no oxidation occurs, the secondary redox parameters (i.e.  $\gamma_{\text{NH}_4}$ ,  $\gamma_{\text{H}_2\text{S}}$ ) are essentially non-influential. Whereas in the oxic scenario, SWI-fluxes of  $\text{NH}_4$ ,  $\text{SO}_4$  and  $\text{H}_2\text{S}$  are very sensitive to changes in the secondary redox parameters. The  $\text{PO}_4$  SWI-flux appears to be insensitive especially under for the oxic condition as the majority is absorbed to Fe-oxides. The sensitivities change if other  $\text{PO}_4$  related equilibrium concentrations  $\text{PO}_4^s$ ,  $\text{PO}_4^a$  and  $M^\infty$  are used (not shown).

To test if OMEN-SED is able to reproduce the magnitude of observed SWI-fluxes, another set of Latin-Hypercube samplings is produced for the two idealised sediment conditions (sample sizes  $N = 3500$ ). Here the two most sensitive parameters  $k_1$  and  $f_1$  and also  $\tilde{k}_2$  are varied, the other parameters are set to their default values (Tables 9 and 10). For the deep sea condition we account for the presence of more refractory OM by sampling  $f_1 \in [0.02, 0.3]$ . Minimum and Maximum values for the other parameters are as in Table 12. The results are compared with a global database of benthic fluxes of  $\text{O}_2$  and  $\text{NO}_3$  (Bohlen et al., 2012). The coloured scatter plots in Figure 7 show that the observed fluxes fall well in the range of SWI-fluxes calculated with OMEN-SED. Also highlighted by the emergence of colour patterns in Figure 7 A+B are the strong interactions between the amount of labile OM  $f_1$  and its degradation rate  $k_1$  for the resulting SWI-fluxes of the most powerful TEA available. In general, a higher degradation rate in combination with more labile OM available leads to a higher SWI-flux.

**DH:** explanation for small P sensitivity correct?

**Table 12.** Range of model parameters used for sensitivity analysis of model predicted output.

Parameter	Description	Units	Minimum	Maximum	Source
$k_1$	labile OM degradation constant	$\text{yr}^{-1}$	$1e^{-4}$	5.0	(1)
$\tilde{k}_2$	order of refractory OM degradation constant ( $k_2 = \tilde{k}_2 \cdot k_1$ )	-	$1e^{-4}$	$1e^{-1}$	(1)
$f_1$	fraction of labile OM	-	0.02	0.98	-
$K_{\text{NH}_4}$	Adsorption coefficient	-	0.8	1.7	(2)
$\gamma_{\text{NH}_4}$	$\text{NH}_4$ fraction oxidised		0.5	1.0	-
$\gamma_{\text{H}_2\text{S}}$	$\text{H}_2\text{S}$ fraction oxidised		0.5	1.0	-
$K_{\text{PO}_4}^{\text{ox}}$	Adsorption coeff. oxic	-	100.0	400.0	(3)
$K_{\text{PO}_4}^{\text{anox}}$	Adsorption coeff. anoxic	-	1.3	2.0	(3)
$k_s$	kinetic P sorption	$\text{yr}^{-1}$	0.1	100.0	(4, 5)
$k_m$	Fe-bound P release	$\text{yr}^{-1}$	0.015	0.02	(4, 5)
$k_a$	authigenic P formation	$\text{yr}^{-1}$	0.001	10.0	(4, 6)

Sources: (1) Arndt et al. (2013); (2): Van Cappellen and Wang (1996); (3): Krom and Berner (1980)  
(4): Gypens et al. (2008); (5): Slomp et al. (1996); (6): Van Cappellen and Berner (1988)

**Table 13.** Model boundary conditions for the two idealised sediment conditions used for the sensitivity analysis (Fig. 6 and 7). All solute concentrations are in nanomole  $\text{cm}^{-3}$ .

Depth (m)	Temp. ( $^{\circ}\text{C}$ )	OC (wt%)	$\text{O}_2$	$\text{NO}_3$	$\text{SO}_4$	$\text{PO}_4$	$z_{\text{bio}}$ (cm)
400	8.0	2.0	0.0	40.0	28,000	40.0	0.001
4000	1.5	1.0	300.0	20.0	28,000	40.0	10.0

### 3.3 Pre-industrial cGENIE coupling and the OM degradation rate

OMEN-SED has been coupled to the global Earth system model cGENIE as described in Section 2.5.2. Our objective is not to perform and discuss a detailed calibration of the two models, as this is beyond the scope of this model development paper. We rather want to showcase, that a coupling is possible and results in general show main sediment features one would expect to see on a global scale. All simulations are run for 20,000 years to steady-state. OMEN-SED is called for each grid-cell in every time step, feeding back the resulting SWI-fluxes and the fraction of POC preserved in the sediments to cGENIE.

Furthermore, the spatial variability in benthic OM degradation kinetics is unknown at the global scale and reported rate constants can vary by almost 10 orders of magnitude (Arndt et al., 2013). Thus, a major challenge for diagenetic models is defining appropriate OM degradation rate constants which is either achieved through profile fitting for a specific site or, for global applications, the rate constants follow empirical relations with a related, readily available sediment characteristic such as water depth (Middelburg et al., 1997), sedimentation rate (Toth and Lerman, 1977; Tromp



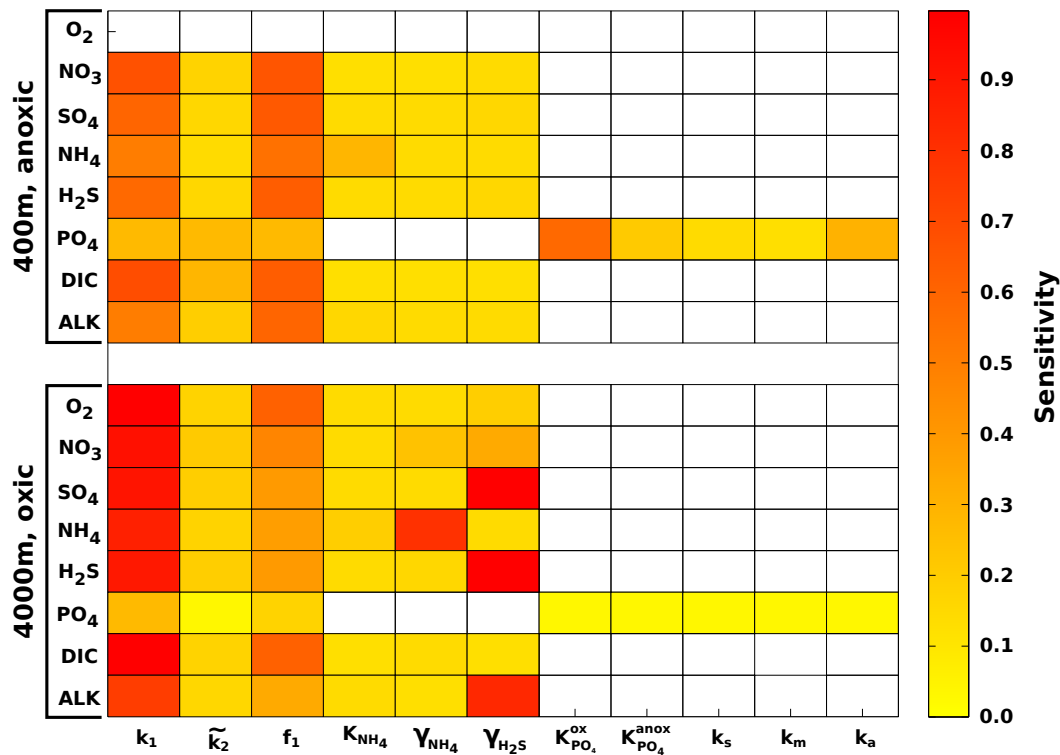
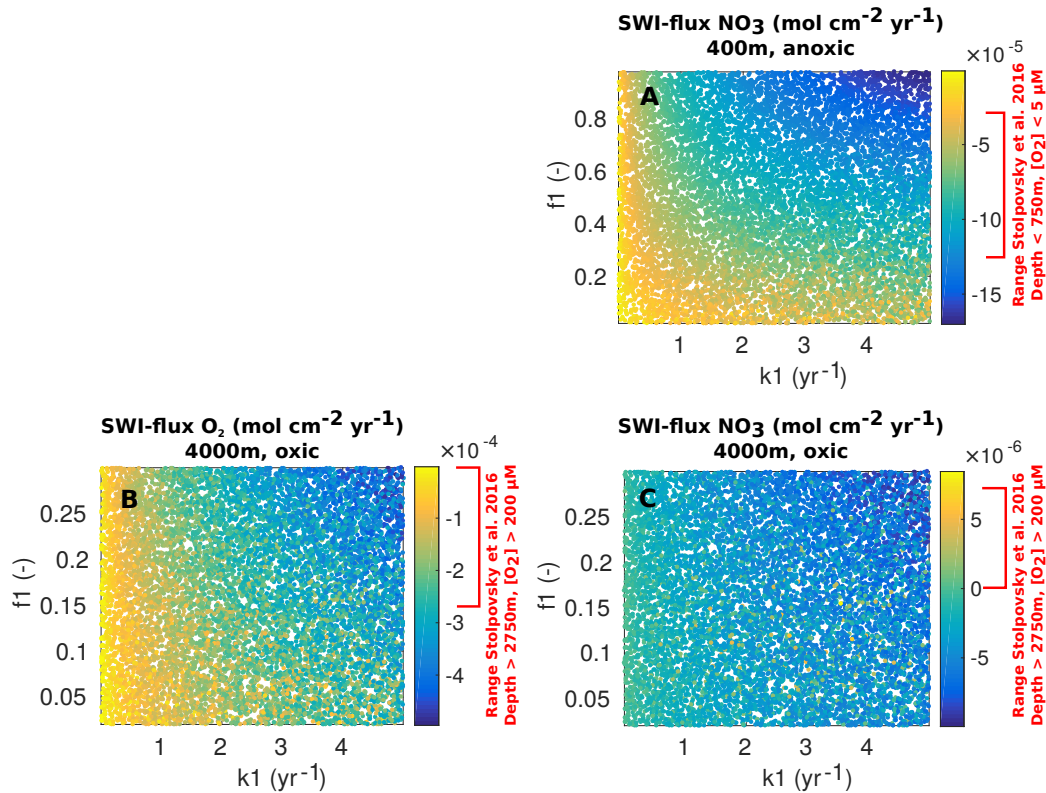


**Figure 6.** Pattern plot, showing the output sensitivity for each SWI flux (i.e. the chemical compounds on the horizontal axis) and each input factor (i.e. the model parameters on the vertical axis) for two idealised sediment cores. White patterns are assigned where the SWI flux is independent of the specific parameter.

**DH:** Rather low  $PO_4$  sensitivity - bc of Equil. concentr.?

*et al.*, 1995) or OM flux (Boudreau, 1997). However, these relationships are mostly based on simple fitting exercises to limited data sets and show at the most a very weak trend and no statistically significant relationship (Arndt et al., 2013). This creates considerable uncertainties when diagenetic models are coupled to global biogeochemical ocean models especially when applying the model for different geological timescales. Other model parameters implicitly accounting for processes not explicitly described are sedimentation and bioturbation rate and are generally related to water depth following Middelburg et al. (1997).

As discussed elsewhere (e.g. Arndt et al., 2013, and references therein) and also shown in our sensitivity analysis 3.2 of all the rate constants the degradation rates of OM ( $k_i$ ) are the most influential parameters and strongly determine the SWI-flux of redox-sensitive elements. Thus, even though it is a major simplification, when coupling a diagenetic model to an ESM it is desirable to relate the OM degradation rates to a single, readily available characteristic (or master variable) of the local environmental conditions. For instance, considerable effort has been expended to relate the apparent rate constant for oxic and anoxic OM degradation to sedimentation rate ( $w$ ) and various empirical rela-



**DH:** Why mainly negative NO<sub>3</sub>-flux 4000m in contrast to database!?

**Figure 7.** Coloured scatter plots ( $k_1$  vs  $f_1$ ) of resulting OMEN-SED SWI-fluxes for the 400m anoxic (A: NO<sub>3</sub>) and 4000m oxic (B: O<sub>2</sub>, C: NO<sub>3</sub>) scenario. Negative values representing a flux from the water column into the sediments. Indicated area in red at the respective colour scale represents the range of benthic fluxes in the global database of Bohlen et al. (2012).

tions have been proposed (Toth and Lerman, 1977; Tromp et al., 1995; Boudreau, 1997; Stolpovsky et al., 2015). We test globally invariant values as well as different published parameterisations for the OM degradation rate constants (see Table 14) to test whether the different approaches are able to recreate main sediment characteristics. Depending on oxygen concentration in the bottom water,  $k_1$  is defined as the oxic or anoxic degradation rate (anoxic for  $[O_2] < 5$  nanomole cm<sup>-3</sup>). The more refractory component is assumed to degrade one hundred times slower ( $k_2 = k_1/100$ , see e.g. Boudreau, 1997).

Describe Figure 8 and compare with what we know. E.g. Thullner et al. 2009!

Schulz and Zabel: The basic mechanism inducing microbial activity is the supply of organic matter to the seafloor and this is generally coupled to surface water productivity. Most of the highly productive areas in the global ocean are adjacent to the continents, so that we can expect a decrease

**Table 14.** List of coupled OMEN-cGENIE experiments with oxic and anoxic rate constants ( $k_1$ ,  $\text{yr}^{-1}$ ). The rate constant  $k_2$  for the more refractory component is calculated as  $k_2 = k_1/100$ , apart from the Control experiment where  $k_2 = 1.0$ .  $D$ : seafloor depth.

Experiment	oxic rate constant	anoxic rate constant	Reference/Description
Control	1.0	1.0	All OM is degraded
Tromp	$2.97 \cdot w^{0.62}$	$0.057 \cdot w^{1.94}$	Tromp et al. (1995)
Boudreau_Toht	$0.38 \cdot w^{0.59}$	$0.04 \cdot w^2$	Boudreau (1997) oxic Toht and Lerman (1977) anoxic
Stolpovsky_Toht	$1.02 \cdot w^{0.5}$	$0.04 \cdot w^2$	Stolpovsky et al. (2015) oxic Toht and Lerman (1977) anoxic
Palastanga	0.01	0.008	$D \leq 2000$
	0.005	0.002	$D > 2000$ Palastanga et al. (2011)

of degradation intensity from the coastal marine environments over the continental shelves and slopes into the deep-sea. This becomes evident when we look at the data compiled by Middelburg et al. (1993) which indicate that 83% mineralization and 87% burial in marine sediments occurs in the coastal zone occupying only 9% of the total ocean area. This means that the sediments with the highest respiration rates also have the highest burial efficiency in marine environments. Fluxes of oxygen and nitrate, therefore, vary over several orders of magnitude between oligotrophic open ocean areas and continental shelf and slope areas. This is about 50 to 6,000  $\text{mmol m}^{-2} \text{yr}^{-1}$  for oxygen and -600 to 380  $\text{mmol m}^{-2} \text{yr}^{-1}$  for nitrate ...

(SHOW O<sub>2</sub>, NO<sub>3</sub> AND E.G. PO<sub>4</sub> SWI-fluxes).

Could also plot Figure 4 from Palastanga et al. (2011) with POC wt% for different sites in the ocean! **UNITS of Fe-P! This is a solid! Therefore not nmol/cm<sup>3</sup> rather mol/g as in Palastanga...**

Also check what water column features to show and maybe sediment P or Fe-P concentrations (see PALASTANGA et al. 2011, 2013).

Stolpovsky: bioturbated sediments deposited at continental margins quickly become anoxic within a few millimeters [Wenzhöfer and Glud, 2002].

#### 4 Scope of applicability and model limitations

Stolpovsky:

- global parameterizations of biologically mediated transport and kinetic processes e.g. bioirrigation and nitrification rates. But no single set of biogeochemical and transport parameters is able to simulate all the shelf sites simultaneously

- globally invariant porosity, in reality permeability of sand is greater than fine-grained mud, such

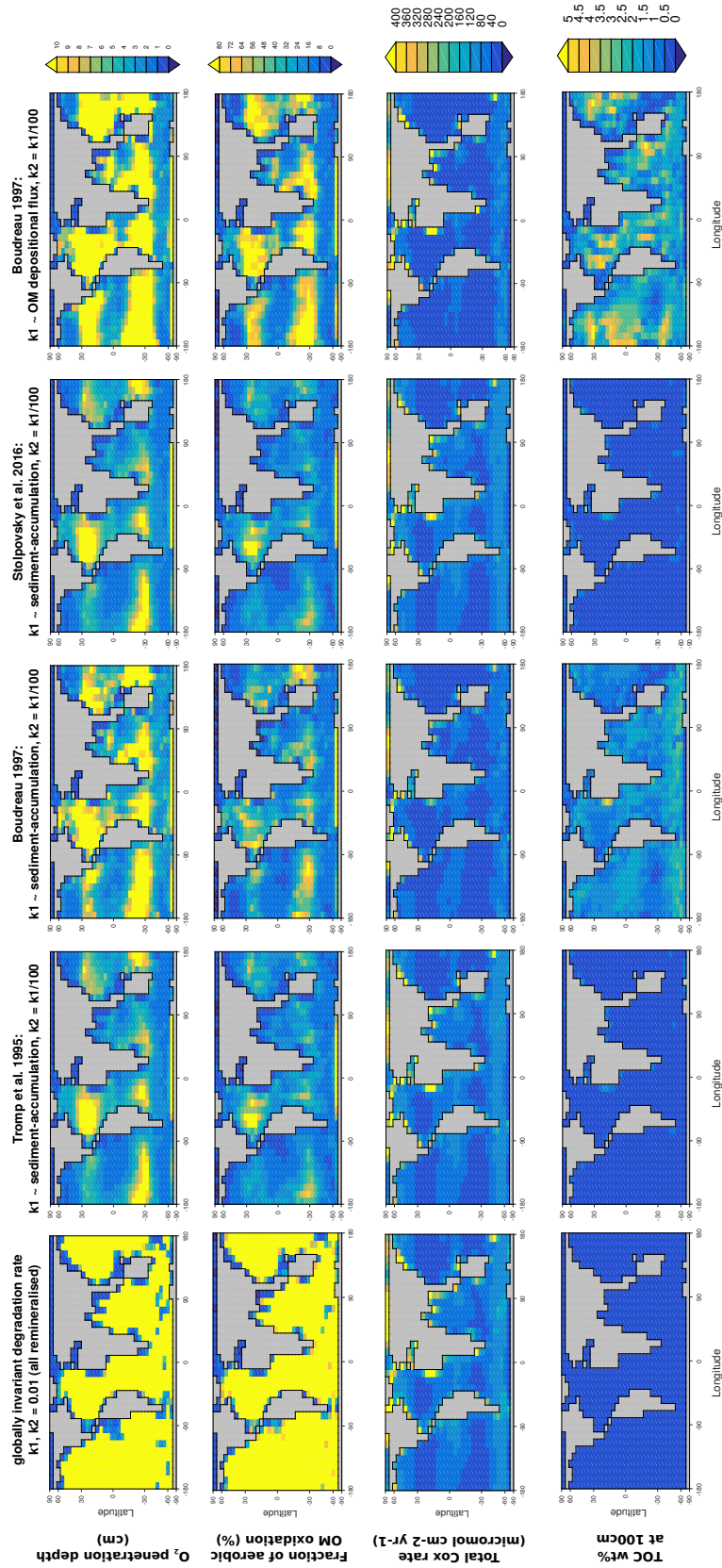


**Figure 8.** Results of OMEN-cGENIE coupling using different, published parameterisations for the OM degradation rates ( $k_1$ ,  $k_2$ , compare Table ??) coupled to the same cGENIE ocean setup. All results shown are sediment characteristics calculated by OMEN-SED. **NOTE: Preliminary results (here frac2 still constant!) TODO: plot wt% just until 3%.**

that boundary layer current and topography interactions will enhance the exchange of pore water with seawater by pressure-driven advective processes [Huettel et al., 1996]. N cycling in sands can thus exhibit large differences compared to fine-grained muds [e.g., Cook et al., 2006; Rao et al., 2007].

- 765 - Not able to simulate site specific seasonal variability in e.g. shallow sediments  
 - no globally realistic parameterisation for k

Schulz and Zabel: also applicable for continental margins or estuaries: Such complex interactions between different pathways of organic matter decomposition and redox reactions are restricted to coastal marine environments and highly accumulating upwelling regions. In oligotrophic regions of the deep sea, 100 to 1,000- times more organic carbon is oxidized by oxygen than by sulfate reduction and other pathways (Canfield 1989).

## 5 Conclusions

Not too bad this model...

## 6 Code Availability

### 775 Appendix A: Reaction Network

### Appendix B: Sensitivity Analysis

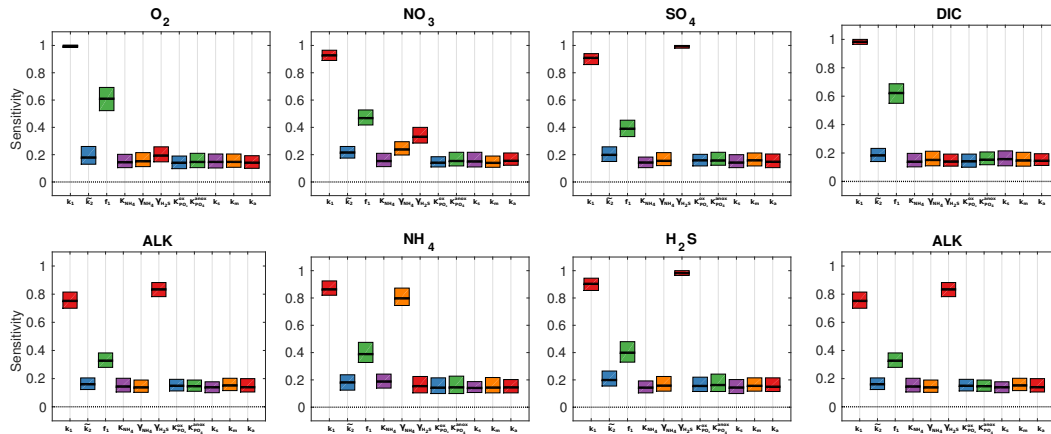


**Figure 9.** Move to Appendix Box plot of parameter sensitivities for the calculated SWI-fluxes for the 4000m oxic condition. Average sensitivities (black lines) and 90% confidence intervals using  $N = 11200$  model evaluations and  $N_{boot} = 100$  bootstrap resamples.

**Table 15.** Primary pathways of organic matter degradation, secondary redox reactions and stoichiometries implemented in the reaction network.

Pathway	Stoichiometry
<b>Primary Redox reactions</b>	
Aerobic degradation	$(\text{CH}_2\text{O})_x(\text{NH}_3)_y(\text{H}_3\text{PO}_4)_z + (\text{x} + 2\text{y})\text{O}_2 + (\text{y} + 2\text{z})\text{HCO}_3^- \rightarrow (\text{x} + \text{y} + 2\text{z})\text{CO}_2 + \text{yNO}_3^- + \text{zHPO}_4^{2-} + (\text{x} + 2\text{y} + 2\text{z})\text{H}_2\text{O}$
Denitrification	$(\text{CH}_2\text{O})_x(\text{NH}_3)_y(\text{H}_3\text{PO}_4)_z + \frac{(4\text{x}+3\text{y})}{5}\text{NO}_3^- \rightarrow \frac{(2\text{x}+4\text{y})}{5}\text{N}_2 + \frac{(\text{x}-3\text{y}+10\text{z})}{5}\text{CO}_2 + \frac{(4\text{x}+3\text{y}-10\text{z})}{5}\text{HCO}_3^- + \text{zHPO}_4^{2-} + \frac{(3\text{x}+6\text{y}+10\text{z})}{5}\text{H}_2\text{O}$
Sulfate reduction	$(\text{CH}_2\text{O})_x(\text{NH}_3)_y(\text{H}_3\text{PO}_4)_z + \frac{\text{z}}{2}\text{SO}_4^{2-} + (\text{y} - 2\text{z})\text{CO}_2 + (\text{y} - 2\text{z})\text{H}_2\text{O} \rightarrow \frac{\text{x}}{2}\text{H}_2\text{S} + (\text{x} + \text{y} - 2\text{z})\text{HCO}_3^- + \text{yNH}_4^+ + \text{zHPO}_4^{2-}$
Methanogenesis	$(\text{CH}_2\text{O})_x(\text{NH}_3)_y(\text{H}_3\text{PO}_4)_z + (\text{y} - 2\text{z})\text{H}_2\text{O} \rightarrow \frac{\text{x}}{2}\text{CH}_4 + \frac{\text{x}-2\text{y}+4\text{z}}{2}\text{CO}_2 + (\text{x} - 2\text{z})\text{HCO}_3^- + \text{yNH}_4^+ + \text{zHPO}_4^{2-}$
<b>Secondary Redox reactions</b>	
Nitrification	$\text{NH}_4^+ + 2\text{O}_2 + 2\text{HCO}_3^- \rightarrow \text{NO}_3^- + 2\text{CO}_2 + 3\text{H}_2\text{O}$
Sulfide oxidation	$\text{H}_2\text{S} + 2\text{O}_2 + 2\text{HCO}_3^- \rightarrow \text{SO}_4^{2-} + 2\text{CO}_2 + 2\text{H}_2\text{O}$
AOM	$\text{CH}_4 + \text{CO}_2 + \text{SO}_4^{2-} \rightarrow 2\text{HCO}_3^- + \text{H}_2\text{S}$
<b>Adsorption reactions and mineral precipitation</b>	
NH <sub>4</sub> adsorption	$\text{NH}_4^+ \xrightarrow{K_{\text{NH}_4}} \text{NH}_4^+(\text{ads})$
P ad-/desorption ???	$\text{PO}_4^{2-} \xrightarrow{K_{\text{PO}_4}^{\text{L,II}}} \text{PO}_4^{2-}(\text{ads}); \quad \text{HPO}_4^{2-} \xrightarrow{k_s} \text{Fe-bound P} \xrightarrow{k_m} \text{HPO}_4^{2-}$
CFA precipitation	$\text{PO}_4^{2-} \xrightarrow{k_a} \text{CFA}$

## **B1**

*Acknowledgements.* Thank you...

## References

- 780 Aguilera, D. R., Jourabchi, P., Spiteri, C., and Regnier, P. (2005). A knowledge-based reactive transport approach for the simulation of biogeochemical dynamics in Earth systems. *Geochemistry, Geophysics, Geosystems*, 6(7).
- Archer, D., Eby, M., Brovkin, V., Ridgwell, A., Cao, L., Mikolajewicz, U., Caldeira, K., Matsumoto, K., Munhoven, G., Montenegro, A., and Tokos, K. (2009). Atmospheric Lifetime of Fossil Fuel Carbon Dioxide.
- 785 *Annual Review of Earth and Planetary Sciences*, 37(1):117–134.
- Archer, D. and Maier-Reimer, E. (1994). Effect of Deep-Sea Sedimentary Calcite Preservation on Atmospheric CO<sub>2</sub> Concentration. *Nature*, 367(6460):260–263. 00506 WOS:A1994MR49400052.
- Archer, D., Winguth, A., Lea, D., and Mahowald, N. (2000). What caused the glacial/interglacial atmospheric pCO<sub>2</sub> cycles? *Reviews of Geophysics*, 38(2):159–189. 00414.
- 790 Archer, D. E., Morford, J. L., and Emerson, S. R. (2002). A model of suboxic sedimentary diagenesis suitable for automatic tuning and gridded global domains. *Global Biogeochemical Cycles*, 16(1):17–1.
- Arndt, S., Jørgensen, B., LaRowe, D., Middelburg, J., Pancost, R., and Regnier, P. (2013). Quantifying the degradation of organic matter in marine sediments: A review and synthesis. *Earth-Science Reviews*, 123:53–86.
- 795 Arthur, M. A., Dean, W. E., and Pratt, L. M. (1988). Geochemical and climatic effects of increased marine organic carbon burial at the Cenomanian/Turonian boundary. *Nature*, 335(6192):714–717.
- Berner, R. A. (1964). An idealized model of dissolved sulfate distribution in recent sediments. *Geochimica et Cosmochimica Acta*, 28(9):1497–1503.
- Berner, R. A. (1980). *Early Diagenesis: A Theoretical Approach*. Princeton University Press.
- 800 Berner, R. A. (1991). A model for atmospheric CO<sub>2</sub> over Phanerozoic time. 291(4):339–376.
- Berner, R. A. (2004). *The Phanerozoic Carbon Cycle: CO<sub>2</sub> and O<sub>2</sub>*. Oxford University Press. 00000.
- Billen, G. (1982). Modelling the processes of organic matter degradation and nutrients recycling in sedimentary systems. *Sediment microbiology*, pages 15–52.
- Bohlen, L., Dale, A. W., and Wallmann, K. (2012). Simple transfer functions for calculating benthic fixed
- 805 nitrogen losses and C:N:P regeneration ratios in global biogeochemical models. *Global Biogeochemical Cycles*, 26(3):GB3029.
- Boudreau, B. P. (1996). A method-of-lines code for carbon and nutrient diagenesis in aquatic sediments. *Computers & Geosciences*, 22(5):479–496.
- Boudreau, B. P. (1997). *Diagenetic models and their implementation*, volume 505. Springer Berlin.
- 810 Boudreau, B. P. (1998). Mean mixed depth of sediments: The wherefore and the why. *Limnology and Oceanography*, 43(3):524–526.
- Boudreau, B. P., Mucci, A., Sundby, B., Luther, G. W., and Silverberg, N. (1998). Comparative diagenesis at three sites on the Canadian continental margin. *Journal of Marine Research*, 56(6):1259–1284.
- Boudreau, B. P. and Ruddick, B. R. (1991). On a reactive continuum representation of organic matter diagenesis.
- 815 *American Journal of Science*, 291(5):507–538. 00187.
- Broecker, W. S. (1982). Ocean chemistry during glacial time. *Geochimica et Cosmochimica Acta*, 46(10):1689–1705.
- Burdige, D. J. (2006). *Geochemistry of marine sediments*, volume 398. Princeton University Press Princeton.



- Canfield, D. E., Kristensen, E., and Thamdrup, B. (2005). *Aquatic Geomicrobiology*. Gulf Professional Publishing.
- Colbourn, G., Ridgwell, A., and Lenton, T. M. (2013). The Rock Geochemical Model (RokGeM) v0.9. *Geosci. Model Dev.*, 6(5):1543–1573.
- Edwards, N. R. and Marsh, R. (2005). Uncertainties due to transport-parameter sensitivity in an efficient 3-D ocean-climate model. *Climate Dynamics*, 24(4):415–433.
- Emerson, S. and Bender, M. L. (1981). Carbon fluxes at the sediment-water interface of the deep-sea: calcium carbonate preservation. *Journal of Marine Research*, 39:139–162.
- Epping, E., van der Zee, C., Soetaert, K., and Helder, W. (2002). On the oxidation and burial of organic carbon in sediments of the Iberian margin and Nazaré Canyon (NE Atlantic). *Progress in Oceanography*, 52(2–4):399–431.
- Goloway, F. and Bender, M. (1982). Diagenetic models of interstitial nitrate profiles in deep sea suboxic sediments. *Limnol. Oceanogr.*, 27(4):624–638.
- Goosse, H., Brovkin, V., Fichet, T., Haarsma, R., Huybrechts, P., Jongma, J., Mouchet, A., Selten, F., Barriat, P.-Y., Campin, J.-M., Deleersnijder, E., Driesschaert, E., Goelzer, H., Janssens, I., Loutre, M.-F., Morales Maqueda, M. A., Opsteegh, T., Mathieu, P.-P., Munhoven, G., Pettersson, E. J., Renssen, H., Roche, D. M., Schaeffer, M., Tartinville, B., Timmermann, A., and Weber, S. L. (2010). Description of the earth system model of intermediate complexity LOVECLIM version 1.2. *Geosci. Model Dev.*, 3(2):603–633.
- Gypens, N., Lancelot, C., and Soetaert, K. (2008). Simple parameterisations for describing n and p diagenetic processes: Application in the north sea. *Progress in Oceanography*, 76(1):89–110.
- Heinze, C., Maier-Reimer, E., Winguth, A. M. E., and Archer, D. (1999). A global oceanic sediment model for long-term climate studies. *Global Biogeochemical Cycles*, 13(1):221–250.
- Hensen, C., Zabel, M., and Schulz, H. N. (2006). Benthic Cycling of Oxygen, Nitrogen and Phosphorus. In Schulz, H. D. and Zabel, M., editors, *Marine Geochemistry*, pages 207–240. Springer Berlin Heidelberg.
- Hülse, D., Arndt, S., Wilson, J., Munhoven, G., and Ridgwell, A. (2017). Understanding the causes and consequences of past marine carbon cycling variability through models. *Earth-Science Reviews*, –:in review.
- Ilyina, T., Six, K. D., Segschneider, J., Maier-Reimer, E., Li, H., and Núñez-Riboni, I. (2013). Global ocean biogeochemistry model HAMOCC: Model architecture and performance as component of the MPI-Earth system model in different CMIP5 experimental realizations. *Journal of Advances in Modeling Earth Systems*, 5(2):287–315.
- Ingall, E. and Jahnke, R. (1994). Evidence for enhanced phosphorus regeneration from marine sediments overlain by oxygen depleted waters. *Geochimica et Cosmochimica Acta*, 58(11):2571–2575. 00302.
- Jahnke, R. A., Emerson, S. R., and Murray, J. W. (1982). A model of oxygen reduction, denitrification, and organic matter mineralization in marine sediments. *Limnol. Oceanogr.*, 27(4):6–10.
- Jarvis, I., Lignum, J. S., Gröcke, D. R., Jenkyns, H. C., and Pearce, M. A. (2011). Black shale deposition, atmospheric CO<sub>2</sub> drawdown, and cooling during the Cenomanian-Turonian Oceanic Anoxic Event. *Paleoceanography*, 26(3):n/a–n/a.
- Jenkyns, H. C. (2010). Geochemistry of oceanic anoxic events. *Geochemistry, Geophysics, Geosystems*, 11(3).
- Jørgensen, B. B. (1978). A comparison of methods for the quantification of bacterial sulfate reduction in coastal marine sediments: II Calculation from mathematical models. *Geomicrobiology Journal*, 1:29–47.

- Jørgensen, B. B. and Kasten, S. (2006). Sulfur Cycling and Methane Oxidation. In Schulz, P. D. H. D. and Zabel, D. M., editors, *Marine Geochemistry*, pages 271–309. Springer Berlin Heidelberg.
- Krom, M. D. and Berner, R. A. (1980). Adsorption of phosphate in anoxic marine sediments1. *Limnology and Oceanography*, 25(5):797–806.
- Lenton, T. M. and Watson, A. J. (2000). Redfield revisited: 1. Regulation of nitrate, phosphate, and oxygen in the ocean. *Global Biogeochemical Cycles*, 14(1):225–248.
- Li, Y.-H. and Gregory, S. (1974). Diffusion of ions in sea water and in deep-sea sediments. *Geochimica et Cosmochimica Acta*, 38(5):703–714.
- Mackenzie, F. T. (2005). *Sediments, Diagenesis, and Sedimentary Rocks: Treatise on Geochemistry, Second Edition*. Elsevier. 00000.
- Meysman, F. J. R., Middelburg, J. J., Herman, P. M. J., and Heip, C. H. R. (2003). Reactive transport in surface sediments. II. Media: an object-oriented problem-solving environment for early diagenesis. *Computers & Geosciences*, 29(3):301–318. 00067.
- Middelburg, J. J., Soetaert, K., and Herman, P. M. (1997). Empirical relationships for use in global diagenetic models. *Deep Sea Research Part I: Oceanographic Research Papers*, 44(2):327–344.
- Mort, H. P., Adatte, T., Föllmi, K. B., Keller, G., Steinmann, P., Matera, V., Berner, Z., and Stüben, D. (2007). Phosphorus and the roles of productivity and nutrient recycling during oceanic anoxic event 2. *Geology*, 35(6):483–486. 00135.
- Munhoven, G. (2007). Glacial–interglacial rain ratio changes: Implications for atmospheric and ocean–sediment interaction. *Deep Sea Research Part II: Topical Studies in Oceanography*, 54(5–7):722–746.
- Najjar, R. G., Jin, X., Louanchi, F., Aumont, O., Caldeira, K., Doney, S. C., Dutay, J.-C., Follows, M., Gruber, N., Joos, F., Lindsay, K., Maier-Reimer, E., Matear, R. J., Matsumoto, K., Monfray, P., Mouchet, A., Orr, J. C., Plattner, G.-K., Sarmiento, J. L., Schlitzer, R., Slater, R. D., Weirig, M.-F., Yamanaka, Y., and Yool, A. (2007). Impact of circulation on export production, dissolved organic matter, and dissolved oxygen in the ocean: Results from Phase II of the Ocean Carbon-cycle Model Intercomparison Project (OCMIP-2). *Global Biogeochemical Cycles*, 21(3):GB3007.
- Palastanga, V., Slomp, C. P., and Heinze, C. (2011). Long-term controls on ocean phosphorus and oxygen in a global biogeochemical model. *Global Biogeochemical Cycles*, 25(3):GB3024.
- Pianosi, F., Beven, K., Freer, J., Hall, J. W., Rougier, J., Stephenson, D. B., and Wagener, T. (2016). Sensitivity analysis of environmental models: A systematic review with practical workflow. *Environmental Modelling & Software*, 79:214–232.
- Pianosi, F., Sarrazin, F., and Wagener, T. (2015). A Matlab toolbox for Global Sensitivity Analysis. *Environmental Modelling & Software*, 70:80–85.
- Pianosi, F. and Wagener, T. (2015). A simple and efficient method for global sensitivity analysis based on cumulative distribution functions. *Environmental Modelling & Software*, 67:1–11.
- Reimers, C. E., Rittenberg, K. C., Canfield, D. E., Christiansen, M. B., and Martin, J. B. (1996). Porewater pH and authigenic phases formed in the uppermost sediments of the Santa Barbara Basin. *Geochimica et Cosmochimica Acta*, 60(21):4037–4057.

- Ridgwell, A. and Hargreaves, J. C. (2007). Regulation of atmospheric CO<sub>2</sub> by deep-sea sediments in an Earth system model. *Global Biogeochemical Cycles*, 21(2):n/a–n/a.
- 900 Ridgwell, A., Hargreaves, J. C., Edwards, N. R., Annan, J. D., Lenton, T. M., Marsh, R., Yool, A., and Watson, A. (2007). Marine geochemical data assimilation in an efficient Earth System Model of global biogeochemical cycling. *Biogeosciences*, 4(1):87–104. 00090.
- Ridgwell, A. and Zeebe, R. E. (2005). The role of the global carbonate cycle in the regulation and evolution of the Earth system. *Earth and Planetary Science Letters*, 234(3–4):299–315. 00172.
- 905 Ruttenger, K. C. (1993). Reassessment of the oceanic residence time of phosphorus. *Chemical Geology*, 107(3):405–409.
- Schulz, H. D. (2006). Quantification of Early Diagenesis: Dissolved Constituents in Pore Water and Signals in the Solid Phase. In Schulz, P. D. H. D. and Zabel, D. M., editors, *Marine Geochemistry*, pages 73–124. Springer Berlin Heidelberg.
- 910 Shaffer, G., Malskær Olsen, S., and Pepke Pedersen, J. O. (2008). Presentation, calibration and validation of the low-order, DCESS Earth System Model (Version 1). *Geosci. Model Dev.*, 1(1):17–51. 00007.
- Slomp, C., Malschaert, J., and Van Raaphorst, W. (1998). The role of adsorption in sediment-water exchange of phosphate in north sea continental margin sediments. *Limnology and Oceanography*, 43(5):832–846.
- Slomp, C. P., Epping, E. H., Helder, W., and Van Raaphorst, W. (1996). A key role for iron-bound phosphorus in authigenic apatite formation in north atlantic continental platform sediments. *Journal of Marine Research*, 915 54(6):1179–1205.
- Soetaert, K., Herman, P. M., and Middelburg, J. J. (1996a). Dynamic response of deep-sea sediments to seasonal variations: a model. *Limnology and Oceanography*, 41(8):1651–1668.
- Soetaert, K., Herman, P. M. J., and Middelburg, J. J. (1996b). A model of early diagenetic processes from the 920 shelf to abyssal depths. *Geochimica et Cosmochimica Acta*, 60(6):1019–1040.
- Soetaert, K., Middelburg, J. J., Herman, P. M. J., and Buis, K. (2000). On the coupling of benthic and pelagic biogeochemical models. *Earth-Science Reviews*, 51(1–4):173–201.
- Stein, R., Rullkötter, J., and Welte, D. H. (1986). Accumulation of organic-carbon-rich sediments in the Late Jurassic and Cretaceous Atlantic Ocean — A synthesis. *Chemical Geology*, 56(1–2):1–32.
- 925 Stolpovsky, K., Dale, A. W., and Wallmann, K. (2015). Toward a parameterization of global-scale organic carbon mineralization kinetics in surface marine sediments. *Global Biogeochemical Cycles*, 29(6):2015GB005087.
- Teal, L., Bulling, M., Parker, E., and Solan, M. (2010). Global patterns of bioturbation intensity and mixed depth of marine soft sediments. *Aquatic Biology*, 2(3):207–218.
- 930 Thullner, M., Dale, A. W., and Regnier, P. (2009). Global-scale quantification of mineralization pathways in marine sediments: A reaction-transport modeling approach. *Geochemistry, Geophysics, Geosystems*, 10(10).
- Tjiputra, J. F., Roelandt, C., Bentsen, M., Lawrence, D. M., Lorentzen, T., Schwinger, J., Seland, Ø., and Heinze, C. (2013). Evaluation of the carbon cycle components in the Norwegian Earth System Model (NorESM). *Geosci. Model Dev.*, 6(2):301–325. 00057.
- 935 Toth, D. J. and Lerman, A. (1977). Organic matter reactivity and sedimentation rates in the ocean. *American Journal of Science*, 277(4):465–485.

- Tromp, T. K., Van Cappellen, P., and Key, R. M. (1995). A global model for the early diagenesis of organic carbon and organic phosphorus in marine sediments. *Geochimica et Cosmochimica Acta*, 59(7):1259–1284. 00164.
- 940 Tsandev, I. and Slomp, C. (2009). Modeling phosphorus cycling and carbon burial during Cretaceous Oceanic Anoxic Events. *Earth and Planetary Science Letters*, 286(1–2):71–79.
- Ullman, W. J. and Aller, R. C. (1982). Diffusion coefficients in nearshore marine sediments. *Limnology and Oceanography*, 27(3):552–556.
- Van Cappellen, P. and Berner, R. A. (1988). A mathematical model for the early diagenesis of phosphorus and  
945 fluorine in marine sediments; apatite precipitation. *American Journal of Science*, 288(4):289–333.
- Van Cappellen, P. and Ingall, E. D. (1994). Benthic phosphorus regeneration, net primary production, and ocean anoxia: A model of the coupled marine biogeochemical cycles of carbon and phosphorus. *Paleoceanography*, 9(5):677–692.
- Van Cappellen, P. and Wang, Y. (1995). Metal cycling in surface sediments: modeling the interplay of transport  
950 and reaction. *Metal contaminated aquatic sediments*, pages 21–64.
- Van Cappellen, P. and Wang, Y. (1996). Cycling of iron and manganese in surface sediments; a general theory for the coupled transport and reaction of carbon, oxygen, nitrogen, sulfur, iron, and manganese. *American Journal of Science*, 296(3):197–243.
- Wang, Y. and Van Cappellen, P. (1996). A multicomponent reactive transport model of early diagenesis: Application to redox cycling in coastal marine sediments. *Geochimica et Cosmochimica Acta*, 60(16):2993–3014.  
955 00283.
- Wolf-Gladrow, D. A., Zeebe, R. E., Klaas, C., Körtzinger, A., and Dickson, A. G. (2007). Total alkalinity: The explicit conservative expression and its application to biogeochemical processes. *Marine Chemistry*, 106(1–2):287–300.